DISSERTATION

On

VOLUMETRIC BRAIN MR IMAGE SEGMENTATION USING ENTROPY BASED FUZZY CLUSTERING ALGORITHM

Thesis Submitted in the partial fulfillment of the requirements for the degree of

Master of Engineering

In

Computer Science & Engineering

Submitted By

SWASTIK BISWAS

Examination Roll number: M4CSE19007

Registration number: 140762 of 2017 − 2018

Under the guidance of

Dr. Jamuna Kanta Sing

Professor, Dept. of Computer Science & Engineering

Faculty Council of Engineering and Technology

JADAVPUR UNIVERSITY

KOLKATA − 700032

2018 − 2019

Faculty Council of Engineering and Technology

JADAVPUR UNIVERSITY, KOLKATA – 700032

Certificate of Recommendation

This is to certify that Swastik Biswas has completed his dissertation entitled "Volumetric Brain MR Image Segmentation using Entropy based Fuzzy Clustering Algorithm, under the supervision and guidance of Prof. (Dr.) Jamuna Kanta Sing, Jadavpur University, Kolkata. We are satisfied with his work, which is being presented for the partial fulfillment of the degree of Master of Engineering in Computer Science & Engineering, Jadavpur University, Kolkata - 700032.
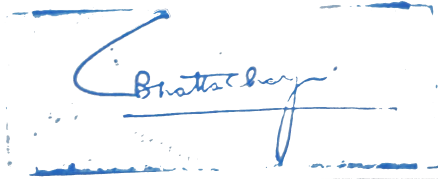
Jamuna Kanta Sing, Ph.D.
Professor
Dept. of Computer Science & Engineering
Jadavpur University, Kolkata-700032

Prof. (Dr.) Jamuna Kanta Sing
Faculty in Charge of Thesis

Prof. (Dr.) Mahantapas Kundu
HOD, Dept. of Computer Science &
Engineering, Jadavpur University,
Kolkata – 700 032

Prof. (Dr.) Chiranjib Bhattacharjee
Dean, Faculty Council of Engineering and
Technology, Jadavpur University,
Kolkata – 700 032

Faculty Council of Engineering and Technology
JADAVPUR UNIVERSITY, KOLKATA – 700032

_Certificate of Approval_*

The foregoing thesis is hereby approved as a creditable study of Master of Engineering in Computer Science & Engineering and presented in a manner satisfactory to warrant its acceptance as a prerequisite to the degree for which it has been submitted. It is understood that by this approval the undersigned do not necessarily endorse or approve any statement made, opinion expressed or conclusion therein but approve this thesis only for the purpose for which it is submitted.

Final Examination for Evaluation of the Thesis

_____ 07/06/19.

_____ Anirudha Dey 07/06/19

Signature of Examiners

* _Only in case the thesis is approved._

Declaration of Originality and Compliance of Academic Ethics

I hereby declare that this thesis contains literature survey and original research work by the undersigned candidate, as part of his Master of Engineering in Computer Science & Engineering.
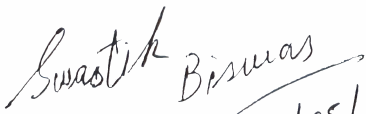
All information in this document has been obtained and presented in accordance with academic rules and ethical conduct.

I also declare that, as required by these rules and conduct, I have fully cited and referenced all material and results that are not original to this work.

Name (Block Letters): SWASTIK BISWAS

Exam Roll Number: M4CSE19007

Thesis Title: VOLUMETRIC BRAIN MR IMAGE SEGMENTATION USING
ENTROPY BASED FUZZY CLUSTERING ALGORITHM

Signature with date:

Acknowledgement

I convey my honest and sincere thanks to my respected teacher and guide *Prof. (Dr.) Jamuna Kanta Sing*, Professor of Department of Computer Science & Engineering, Jadavpur University, for his exclusive guidance and undivided support in completing and presenting this thesis successfully. I am indebted to him for the constant encouragement and continuous inspiration that he has given me. The above words are only a token of my deep respect towards him for all that he has done to take my thesis to its present shape.

I would also like to thank *Mrs. Nabanita Mahata* for her valuable suggestions and key insights that she has provided while working on this thesis.

Finally, I express my sense of gratitude and thanks to my family members, especially my parents for their unconditional love and support. Last but not the least I am grateful to all my friends for staying beside me and being an endless source of optimism and positive thoughts.

Contents

List of Figures

List of Tables

Abstract

In this dissertation entitled "Volumetric Brain MR Image Segmentation using Entropy based Fuzzy Clustering Algorithm" an image segmentation method has been proposed that is based on fuzzy c-means algorithm and has been modified by using Shannon entropy to improve the robustness to the noise and intensity inhomogeneity that may be present in a brain MR image. A very detailed comparative analysis has made with different use cases also including a contrast with earlier methods.

Chapter 1:

Introduction

1.1 Fuzzy image segmentation

Image segmentation is a method of segregating a digital image into various elements that can be referred to as sets of pixels, or super-pixels. The objective of segmentation is to clarify and/or modify the illustration of a picture into one thing that holds additional meaningful information and is easier to research [1]. Image segmentation is usually applied in order to find objects and bounds (lines, curves, etc.) in pictures. In exact terms, image segmentation is the method of assignment of a label to each element in an image in such a way that the specified pixels with constant label share bound characteristics.

The results of image segmentation may be a set of contours extracted from the image. In any region each pixel bear similarity with reference to some characteristic or computed property, like color, intensity, or texture. Adjacent regions are considerably different with reference to the constant characteristic(s) [1]. Image Segmentation has two major goals. The initial aim being fragmenting the image into elements for additional analysis. The subsequent intent is to carry out a change of presentation [1].

There are various techniques that have been developed for image segmentation and overall image segmentation approaches can be divided into four categories: thresholding, clustering, edge detection, and region extraction. Many clustering methods are used, like the crisp clustering theme and also the fuzzy clustering theme, each of which has its own special characteristics [2].

Fuzzy set theory, which involves the idea of partial membership described by a membership function, fuzzy clustering (also known as soft clustering) has been widely studied and successfully applied to a variety of applications of image segmentation

including pattern recognition, object detection, and medical imaging. Among the fuzzy clustering strategies, fuzzy c-means (FCM) algorithmic rule is the most well-liked methodology utilized in image segmentation as a result of its strong characteristics for ambiguity and may retain abundant more information than hard segmentation methods [2]. Also, FCM clustering could show a transition zone between clusters and reflect gradual changes in environmental parameters. This is because fuzzy classes contain more information than discrete classes that helps to improve analysis [3].

1.2   Brain MR image segmentation

In brain MR (magnetic resonance) image analysis, image segmentation is commonly used for measuring and visualizing the brain's anatomical structures for analyzing brain changes identifying pathological regions and for surgical planning and image guided intervention. Any kind of abnormalities could be identified by tracking of changes in volume, shape and regional distribution of brain tissue.

Furthermore, brain image segmentation plays an important role in clinical diagnostic tools, treatment procedures and also 3D brain visualization for measuring the volume of different tissues in brain such as Gray and White Matter, Thalamus, Amygdala, Hippocampus etc. [4]. Because, some people modify the problem to a three-type tissue classification by assuming multiple gray matter structures as one class, they usually label the brain volumes into three main classes like White matter (WM), Grey matter (GM), Cerebrospinal fluid (CSF) [4]. The Internet Brain Segmentation Repository (IBSR) provided by the Center for Morphometric Analysis (CMA) at Massachusetts General Hospital and BrainWeb, which has been collected at McConnell Brain Imaging Centre of the Montreal Neurological Institute, McGill University are two popular datasets generally used in this domain of research [4].
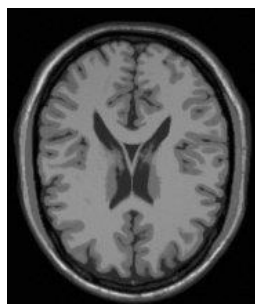
Figure 1.1(a): 2D MR brain image   Figure 1.1(b): 3D MR brain image
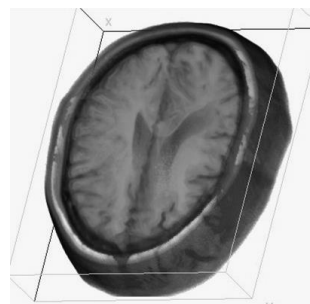
A 2D image can be defined as a function $I(i, j)$ in 2D space where $i = 0, 1, 2, \ldots, M - 1$, $j = 0, 1, 2, \ldots, N - 1$ denotes spatial coordinates. The values of the function $I(i, j)$ are the intensity values and typically represented by a grey value $[0 - 255]$ in MR of the brain [5]. Every image consists of a finite set of image elements, called pixels in 2D-space. Each image element is uniquely specified by its intensity values and its coordinates, (i, j) for pixels where i is image row and j is the column number [5].

A 3D image can be defined as a function $I(i, j, k)$ in 3D space where $i = 0, 1, 2, \ldots, M - 1$, $j = 0, 1, 2, \ldots, N - 1$ denotes spatial coordinates and $k = 0, 1, 2, \ldots, P - 1$ represents each 2D image slice of the 3D image. The values (i, j) of the function $I(i, j, k)$ are the intensity values and typically represented by a grey value $[0 - 255]$ in MR of the brain whereas the k value is represented by any real number $[0 - (P - 1)]$ in which P is the total number of slices of 2D images in the 3D volumetric stack [5].
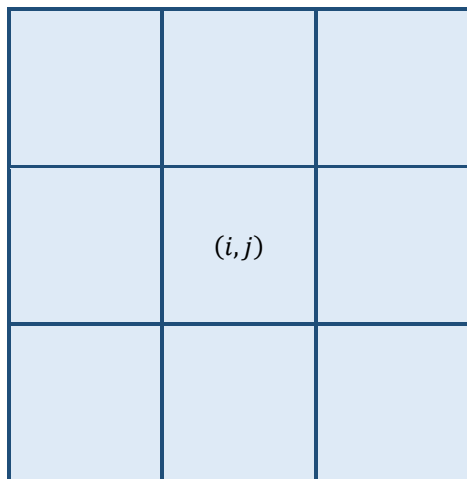
Figure 1.2(a): 2D image representation   *Figure 1.2(b): 3D image representation*
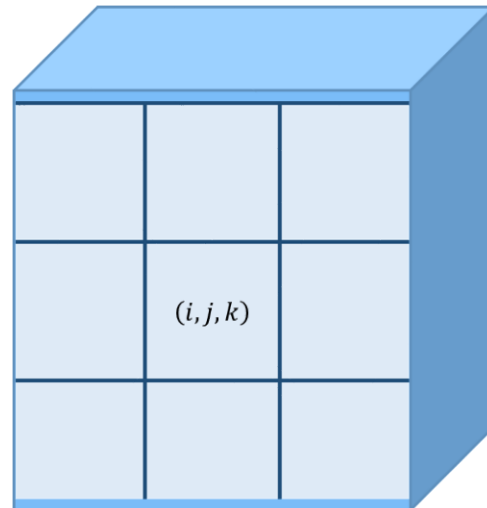
As mentioned earlier in this case of brain MR image elements are typically classified into three main tissue types: CSF, GM, WM. Most of the image segmentation methods are focused on 2D-images while a few are focused 3D-volumes of images.

Chapter 2:

Literature Survey

2.1 Types of segmentation methods

There are a number of segmentation methods of medical images such as, MR images used popularly in the past. Intensity thresholding, region-based segmentation, edge-based segmentation and classification-based segmentation are such techniques which have been used regularly for segmenting MR images [5-7].

The grey level histogram of the image is considered as the threshold level in Intensity thresholding. The disadvantage of intensity thresholding method is that we need to determine the optimal threshold also another disadvantage of intensity thresholding method is spatial uncertainty as the pixel location information is ignored [8].

In the edge-based segmentation technique, interrupted or scattered contour lines are created around an object of interest using some edge detection algorithms. Then these contour lines joined based on some similarity criteria to detect the object of ROI. However, these methods are computationally expensive for obtaining hole free segmentation of the objects. The region-based segmentation methods extend the thresholding by integrating it with connectivity by means of an intensity similarity measure. The major objective of these above-mentioned methods is to get connected regions based on homogeneity criteria of neighborhood pixels. These are sensitive to noise [9] and less suitable for medical image segmentation.

In classification-based segmentation method, the FCM clustering algorithm [10], is more efficient than other hard clustering methods, like k-means algorithm etc. The FCM algorithm is more reasonable in real applications because it allows pixels to

have relation with multiple clusters with varying degree of memberships. FCM is no doubt a very popular unsupervised clustering method, but it has some serious disadvantages due to consideration of the image spatial information. It has another drawback of local optimal solution due to poor initialization. Many modified fuzzy clustering approaches have been reported in the past for making the FCM algorithm more robust to noise and outliers for image segmentation [11-27].

Pedrycz [11] introduced a conditional FCM based clustering method guided by an auxiliary or conditional variable. The method reveals a structure within a group of patterns by considering their vicinity in a feature space along with the similarity of the values assumed by a certain conditional variable. Mohamed et al. [13] modified the FCM algorithm through the incorporation of the spatial information. They introduced the spatial information into the computation of similarity measure. The similarity measure is modified to drag a pixel closure to the cluster center if it is in homogenous region. The drawbacks of this algorithm are its sensitivity to the non-descriptive initial clusters and its massive computational loads.

Ahmed et al. [14] introduced the local grey level information by modifying the objective function with another similarity measure for bias field estimation and segmentation of MRI data. This method is also expensive in terms of computation time. Many researchers subsequently modified the objective functions and develop several robust FCM variants for image segmentation [15-22]. These algorithms are shown to have better performances than the standard FCM algorithm. However, some of these methods depend on a fixed spatial factor which needs to be adjusted according to the real applications. In order to overcome the problem of over-smoothed edges, use of larger spatial window, adaptive selection mechanisms of the spatial parameters have been proposed [23-25]. The performance of these methods are superior and are able to reduce partly the blurring effects which arise due to use of filtering and larger spatial window. Another major contribution with spatial information into the FCM membership function was suggested by Chuang et al. [26], known as spatial FCM (sFCM) algorithm. The spatial function is the summation of the membership function in the neighborhood of each pixel under consideration. It represents the probability for a pixel to belong into a particular cluster. This spatial function is incorporated into a weighted membership function. The advantages of this method are, it yields regions more homogenous than those of other methods and it removes the noisy spots and partly reduces the spurious blobs.

Recently Qiu et al. [27] suggested a novel algorithm for fuzzy segmentation by introducing two fuzzifiers and a spatial constraint in the membership function. Benaichouche et al. [28] presented another improvement of the FCM clustering algorithm using PSO, Mahalanobis distance and post segmentation correction. The first step introduced PSO initialization to overcome the problem of local minima in

the solution, the second step was concerned with the integration of the spatial gray level information and the Mahalanobis distance and the final step refined the segmentation results by reallocating the potentially misclassified pixels. Kannan et al. [29] introduced a class of robust non–Euclidean distance measure for the objective function to enhance the robustness of the original FCM clustering algorithm and to reduce noise and outliers. Liao et al. [30] proposed a fast-spatial constrained fast kernel based fuzzy c-means clustering (FKFCM) algorithm for MR brain image segmentation. The FKFCM algorithm first transforms the pixel intensities into a higher dimensional space using a kernel trick and then performs classification on the transformed data.

Selvathi et al. [31] presented a modified version of the spatial FCM algorithm to classify the pixels. Adhikari et al. [32] presented a method for MRI brain image segmentation by incorporating intensity inhomogeneity and spatial information by using probabilistic FCM algorithm. The method works in two steps. First it estimates the intensity inhomogeneity or bias field in the MR medical images. The intensity inhomogeneity or intensity non-uniformity usually refers to the slow, non-anatomic intensity variations of the same tissue over the image domain and causes due to imperfection of the image acquisition devices, eddy current, poor magnetic field and patient movement etc. Then the inhomogeneity is corrected by using fusion of suitable Gaussian surfaces which are obtained from calculating the gradient map of different homogenous regions. After this process the corrected image is segmented using a modified probabilistic FCM clustering algorithm that takes into consideration the spatial features of pixels of the image.

Chapter 3:

Proposed Method – Volumetric Brain MR Image Segmentation using Entropy based Fuzzy Clustering Algorithm

3.1 Concept

In our proposed method we incorporate Shannon entropy with conventional FCM algorithm that can effectively segment brain MR images with the presence of noise and intensity inhomogeneity. Entropy is involved as the dissimilarity among the pixels in the regions along the edges is very high.

Entropy was first introduced in thermodynamics developing an information theoretical concept which is closely connected to the internal energy of the system. It has significant applications in physics, information theory, mathematics and other branches of science and engineering [33]. Entropy is the measure of the degree of uncertainty that can be used to characterize the texture of the input image.

Entropy is formulated as follows [34, 46]:

$$ -\sum p_i \times \log p_i \qquad\qquad \text{... (3.1)} $$

where p_i is the probability of a given symbol.

There are different kinds of entropies with significant applications. Some of them are discussed as follows:

3.1.1   Shannon Entropy

Shannon entropy provides an absolute limit on the best possible lossless compression of a signal under constraint. It is denoted by $H_s(p_{m1m2})$ and defined as [34, 38]

$$H_s(P_{m1m2}) = -\sum_{m1}\sum_{m2} p_{m1m2} \log p_{m1m2} \qquad \text{... (3.2)}$$

where p_{m1m2} is the probability density function in 2D random variable [35] where $m1, m2$ are the two dimensions of measuring.

3.1.2   Rényi entropy

It generalizes the Shannon entropy and is important in quantum information where it can be used as a measure of entanglement. It is defined as the entropy of the order of α, where $\alpha \geq 0$ and $\alpha \neq 1$, is constructed as [34, 38]

$$H_r(p_{m1m2}) = \frac{1}{1-\alpha} \log \sum_{m1}\sum_{m2} (p_{m1m2})^\alpha \qquad \text{... (3.3)}$$

Sadek et al. [36] suggested an efficient and fast entropy-based method for noisy cell image segmentation based on generalized α – entropy by measuring the maximum structural information of the image and locating the optimal threshold desired by the segmentation. They mentioned that chief advantages of their proposed methods are its high rapidity and its tolerance to presence of noise in the image.

3.1.3   Harvrda – Charvet

This entropy is used for statistical physics and modified by Dracozy. This can be identified as the function of α and can be represented in the following mathematical form [34, 38]

$$H_{hc}(p_{m1m2}) = \frac{1}{2^{\alpha-1}} \sum_{m1}\sum_{m2} p_{m1m2}^\alpha - 1 \qquad \text{... (3.4)}$$

3.1.4　Kapur entropy

This entropy is denoted by $H_k(\rho_{m1m2})$ of order of α and type β, is represented as [34, 37, 38]

$$H_k(p_{m1m2}) = \left(\frac{\sum_{m1}\sum_{m2} p_{m1m2}^{\alpha+\beta-1}}{\sum_{m1}\sum_{m2} p_{m1m2}^{\beta}}\right)(2^{1-\alpha}-1)^{-1} \qquad \text{... (3.5)}$$

3.1.5　Vajda entropy

It is a special case of Kapur entropy where $\beta = 1$ is taken and Vajda measures $H_v(p_{m1m2})$. It is preferred over Kapur entropy as its calculations are faster and is defined as follows [34, 38]

$$H_k(p_{m1m2}) = \left(\frac{\sum_{m1}\sum_{m2} p_{m1m2}^{\alpha}}{\sum_{m1}\sum_{m2} p_{m1m2}}\right)(2^{1-\alpha}-1)^{-1} \qquad \text{... (3.6)}$$

3.2　Problem Analysis

As MR images are sensitive to noise [9] and intensity inhomogeneity, it is very difficult to achieve effective results. So, to detect diseased regions in MR images, it is necessary to segment the image into different tissue regions (CSF, GM, WM) accurately. To improve the robustness of the conventional FCM algorithm we incorporate Shannon entropy in our proposed method. As entropy is proportional to uncertainty, our goal is to minimize the entropy to obtain better segmented output. The proposed method allows to partition the image pixels by calculating the centers of clusters, v_i and the membership matrix, U through minimizing the following objective function, with respect to these clusters and membership values in an iterative manner.

$$J = \sum_{i=1}^{C}\sum_{k=1}^{N}[\alpha\mu_{ik}^{m}d_{ik}^{2} + (1-\alpha)P_{ik}^{m}d_{ik}^{2}] - \sum_{i=1}^{C}\sum_{k=1}^{N}P_{ik}\ln(P_{ik}) \qquad \text{... (3.7)}$$

subject to the constraint,

$$\sum_{j=1}^{C} \mu_{jk} = 1 \qquad\qquad \text{... (3.8)}$$

where,

$$d_{ik}^2 = \|x_k - v_i\|^2 \qquad\qquad \text{... (3.9)}$$

$$P_{ik} = \frac{G_{ik}}{\sum_{i=1}^{C} G_{lk}} \qquad\qquad \text{... (3.10)}$$

$$G_{ik} = \frac{e^{\frac{-\|x_k - v_i\|^2}{2\sigma_i^2}}}{\sum_{l=1/x_l \in N_k}^{N_k} e^{\frac{-\|x_k - v_i\|^2}{2\sigma_i^2}}} \qquad\qquad \text{... (3.11)}$$

where C is the total number of clusters, N is the number of patterns, α is a parameter (> 0), m is the fuzzifier (> 1). In our proposed method the value of m has been set different for different experiments after a thorough comparative analysis (explained in the next chapter). μ_{ik} is the degree of fuzzy membership of pixel x_k in the ith cluster, d_{ik}^2 represents the Euclidean distance between the cluster center v_i and pixel x_k, $\|*\|$ is any norm expressing the similarity between any measured data and the center and $-\sum_{i=1}^{C}\sum_{k=1}^{N} P_{ik} \ln(P_{ik})$ is the Shannon entropy. $e^{\frac{-\|x_k - v_i\|^2}{2\sigma_i^2}}$ denotes the Gaussian distance between pixel x_k and cluster center v_i. G_{ik} is the ratio of Gaussian distance of pixel x_k with respect to its neighborhood group.

Minimizing the objective function (3.7) with respect to the constraint $\sum_{i=1}^{C} \mu_{ik} = 1$, we obtain

$$\frac{\partial}{\partial \mu_{ik}}(J) = 0 \qquad\qquad \text{... (3.12)}$$

$$\frac{\partial}{\partial v_i}(J) = 0 \qquad\qquad \text{... (3.13)}$$

Differentiating the equation (3.7) partially with respect to μ_{ik}, we get the following equation:

$$\frac{\partial}{\partial \mu_{ik}}(J) = \alpha m \mu_{ik}^{m-1} d_{ik}^2 - \lambda_l \qquad\qquad \text{... (3.14)}$$

From equation **(3.7)** and **(3.12)** we get

$$\alpha m \mu_{ik}^{m-1} d_{ik}^2 - \lambda_l = 0 \qquad \qquad \text{… (3.15)}$$

$$\mu_{ik} = \left[\frac{\lambda_l}{\alpha m d_{ik}^2} \right]^{\frac{1}{m-1}} \qquad \qquad \text{… (3.16)}$$

Using equation **(3.8)**, $\sum_{j=1}^{C} \mu_{jk} = 1$, we get

$$\sum_{j=1}^{C} \left[\frac{\lambda_l}{\alpha m d_{jk}^2} \right]^{\frac{1}{m-1}} = 1 \qquad \qquad \text{… (3.17)}$$

Or,

$$\left[\frac{\lambda_l}{m\alpha} \right]^{\frac{1}{m-1}} = \frac{1}{\sum_{j=1}^{C} \left[\frac{1}{d_{jk}^2} \right]^{\frac{1}{m-1}}} \qquad \qquad \text{… (3.18)}$$

From **(3.16)** and **(3.18)**, we get

$$\mu_{ik} = \frac{1}{\left[\frac{d_{ik}^2}{\sum_{j=1}^{C} d_{jk}^2} \right]^{\frac{1}{m-1}}} \qquad \qquad \text{… (3.19)}$$

Similarly, deriving equation **(3.7)** partially with respect to v_i, we get the following equation

$$\begin{aligned}
\frac{\partial}{\partial v_i}(J) = \sum_{k=1}^{N} &\left[\alpha \mu_{ik}^m \frac{\partial}{\partial x}(d_{ik}^2) + (1-\alpha) P_{ik}^m \left(\frac{\partial}{\partial x}(d_{ik}^2) \right) \right. \\
&\left. + (1-\alpha) \left(\frac{\partial}{\partial x}(P_{ik}^m) \right) d_{ik}^2 \right] \\
&- \sum_{k=1}^{N} \left[\left(\frac{\partial}{\partial x}(P_{ik}) \right) \ln P_{ik} + P_{ik} \left(\frac{\partial}{\partial x}(\ln P_{ik}) \right) \right] \qquad \text{… (3.20)}
\end{aligned}$$

For solving the equation **(3.20)**, we need to find the derivatives of P_{ik} and d_{ik}^2 and then use those values as per chain rule of Calculus.

Therefore, upon deriving equation **(3.9)** we get,

$$\frac{\partial}{\partial \mu_{ik}}(d_{ik}^2) = -2\|x_k - v_i\| \qquad \qquad \text{... (3.21)}$$

Or,

$$\frac{\partial}{\partial \mu_{ik}}(d_{ik}^2) = -2d_{ik} \qquad \qquad \text{... (3.22)}$$

And on deriving equation (3.10) we get,

$$\frac{\partial}{\partial \mu_{ik}}(P_{ik}) = \frac{\sum_{l=1}^{C} G_{lk} \frac{\partial}{\partial v_i}(G_{ik}) - G_{ik} \frac{\partial}{\partial v_i}(\sum_{l=1}^{C} G_{lk})}{(\sum_{l=1}^{C} G_{lk})^2} \qquad \qquad \text{... (3.23)}$$

$$\frac{\partial}{\partial v_i}(G_{ik}) = \left[\frac{(x_k - v_i) - \sum_{l=1/x_l \in N_k}^{N_k}(x_l - v_i)}{\sigma_i^2}\right] G_{ik} \qquad \qquad \text{... (3.24)}$$

$$\frac{\partial}{\partial \mu_{ik}}(P_{ik}) = \frac{\left[(x_k - v_i) - \sum_{l=1/x_l \in N_k}^{N_k}(x_l - v_i)\right] G_{ik}}{\sigma_i^2 \sum_{l=1}^{C} G_{lk}} \qquad \qquad \text{... (3.25)}$$

Or,

$$\frac{\partial}{\partial \mu_{ik}}(P_{ik}) = \frac{[(x_k - v_i) - (\overline{x_l - v_l})] G_{ik}}{\sigma_i^2 \sum_{l=1}^{C} G_{lk}} \qquad \qquad \text{... (3.26)}$$

The term $\sum_{l=1/x_l \in N_k}^{N_k}(x_l - v_i)$ represents the neighborhood of the pixel value with respect to its cluster center. This has been represented by $\overline{x_l - v_l}$ in the equations. While calculating the neighborhood we have again made a very detailed comparative analysis that is covered in the following chapter.

From (3.13) and (3.20) we get

$$\sum_{k=1}^{N} \left[-2\alpha\mu_{ik}^m d_{ik} - 2(1-\alpha)P_{ik}^m d_{ik} \right.$$

$$+ m(1-\alpha)P_{ik}^{m-1} \left\{ \frac{\left(\left(d_{ik} - \overline{d_{ll}}\right)\right) G_{ik}}{\sigma_i^2 (\sum_{l=1}^{C} G_{lk})} \right\} d_{ik}^2 \right]$$

$$- \sum_{k=1}^{N} \left[\left\{ \frac{(d_{ik} - \overline{d_{ll}}) G_{ik}}{\sigma_i^2 (\sum_{l=1}^{C} G_{lk})} \right\} \ln P_{ik} + \left\{ \frac{\left(\left(d_{ik} - \overline{d_{ll}}\right)\right) G_{ik}}{\sigma_i^2 (\sum_{l=1}^{C} G_{lk})} \right\} \right] = 0 \qquad \text{... (3.27)}$$

Using the values from (3.22) and (3.26) in equation (3.27) and simplifying we finally get the following equation

$$v_i = \left[\frac{f(A)}{f(B)}\right] \qquad \text{... (3.28)}$$

where $f(A)$ and $f(B)$ are defined as follows

$$
\begin{aligned}
f(A) = \sum_{k=1}^{N} \Bigg[& 2\alpha\mu_{ik}^m x_k + 2(1-\alpha)P_{ik}^m x_k + \frac{(1-\alpha)d_{ik}^2 x_k G_{ik}}{\sigma_i^2(\sum_{l=1}^{C} G_{lk})} \\
& -\frac{(1-\alpha)\bar{x}_l d_{ik}^2 G_{ik}}{\sigma_i^2(\sum_{l=1}^{C} G_{lk})} + \frac{x_k G_{ik} \ln P_{ik}}{\sigma_i^2(\sum_{l=1}^{C} G_{lk})} - \frac{\bar{x}_l G_{ik} \ln P_{ik}}{\sigma_i^2(\sum_{l=1}^{C} G_{lk})} \\
& + \frac{x_k G_{ik}}{\sigma_i^2(\sum_{l=1}^{C} G_{lk})} - \frac{\bar{x}_l G_{ik}}{\sigma_i^2(\sum_{l=1}^{C} G_{lk})} \Bigg]
\end{aligned}
\qquad \text{... (3.29)}
$$

$$
\begin{aligned}
f(B) = \sum_{k=1}^{N} \Bigg[& 2\alpha\mu_{ik}^m + 2(1-\alpha)P_{ik}^m + \frac{(1-\alpha)d_{ik}^2 G_{ik}}{\sigma_i^2(\sum_{l=1}^{C} G_{lk})} \\
& -\frac{N_k(1-\alpha)d_{ik}^2 G_{ik}}{\sigma_i^2(\sum_{l=1}^{C} G_{lk})} + \frac{G_{ik} \ln P_{ik}}{\sigma_i^2(\sum_{l=1}^{C} G_{lk})} - \frac{N_k G_{ik} \ln P_{ik}}{\sigma_i^2(\sum_{l=1}^{C} G_{lk})} \\
& + \frac{G_{ik}}{\sigma_i^2(\sum_{l=1}^{C} G_{lk})} - \frac{N_k G_{ik}}{\sigma_i^2(\sum_{l=1}^{C} G_{lk})} \Bigg]
\end{aligned}
\qquad \text{... (3.30)}
$$

Based on the above derivations we have carried out extensive evaluation and analysis on both BrainWeb and IBSR dataset followed by test cases on the MR images of real patients. In all of the tests that we have executed there are various quantitative evaluation metrics that have been used and they are defined in succession.

3.3   Quantitative Evaluation Metrics

For comparative study quantitative evaluation is essential. We have presented three types of quantitative evaluation based on

i.   Cluster validity functions
ii.   Segmentation accuracy
iii. Tissue segmentation accuracy

The cluster validity functions are presented in terms of

(a) Partition coefficient
(b) Partition entropy
(c) Similarity index

To reduce the influence of the selected images, results are

3.3.1   Cluster Validity Functions

(a)   Partition Coefficient $\left(V_{pc}\right)$:

Partition coefficient is one of the most important indicators of fuzzy partition and provides best performance with less fuzziness when the value of V_{pc} takes its optimal value as 1, with higher values being "better". It can be represented as follows [25, 27, 42]:

$$V_{pc} = \frac{\sum_{i=1}^{C} \sum_{k=1}^{N} \mu_{ik}^2}{N} \qquad \qquad \text{... (3.31)}$$

(b)   Partition Entropy $\left(V_{pe}\right)$:

Partition entropy is another important indicator of fuzzy partition. To achieve best clustering the value of V_{pe} should be minimal and its value is 0, with higher values being "better". It can be defined as follows [25, 27, 43]:

$$V_{pe} = \frac{-\sum_{i=1}^{C} \sum_{k=1}^{N} [\mu_{ik}^2 \log \mu_{ik}^2]}{N} \qquad \qquad \text{... (3.32)}$$

(c)   Similarity Index (ρ):

Let for an image with C clusters, if A_i and B_i represent the set of pixels belonging to a cluster i in the segmented image and in the "ground truth" image respectively, then the similarity index ρ is stated as follows [6]:

$$\rho = \frac{1}{C} \sum_{i=1}^{C} \left[\frac{2|A_i \cap B_i|}{|A_i| + |B_i|} \right] \times 100\% \qquad \qquad \text{... (3.33)}$$

The value of similarity index is ranged in $[0, 1]$ and the optimal clustering result is achieved when $\rho = 1$, with higher value being "better". It is a very efficient validity measurement as it compares the segmentation results with the ground truth. Noise and inhomogeneity free image is considered here as the ground truth image.

3.3.2   Segmentation Accuracy (SA)

SA is defined as the sum of the correctly classified pixels divided by the sum of the total number of pixels of the clustered image. It can be represented as follows [6]:

$$SA = \frac{n\left(A_j \cap C_j\right)}{n\left(C_j\right)} \qquad \text{... (3.34)}$$

In the above expression, A_j is the set of pixels belonging to the jth cluster found by the proposed method, C_j is the set of pixels of the jth cluster in the ground truth image and $n(*)$ represents the cardinality of the set. For an ideal result, the value of SA will be 1, with higher values being "better".

3.3.3   Tissue Segmentation Accuracy (TSA)

This is defined as follows [6]:

$$TSA = \frac{2N_{CTK}}{N_{CITK} + N_{GTK}} \qquad \text{... (3.35)}$$

In the above definition, N_{CTK} denotes the number of pixels that are correctly assigned to tissue k by the proposed method. N_{CITK} is the total number of pixels assigned to tissue k and N_{GTK} is the number of pixels belonging to tissue k in the ground truth. For an ideal result, TSA will be 1, with higher values being "better".

Chapter 4:

Experimental Results

The performance of the proposed method is first evaluated on the BrainWeb [39] dataset specifically on the simulated T1-weighted images and simulated T2-weighted images followed by IBSR [40] dataset and later on real patient images of human brain in both quantitative and qualitative manner.

The performance of the proposed method is first examined by changing the neighborhood values with the fuzziness coefficient (m) from which we conclude the best possible results. Then it is followed by a comparative study with FCM [45], FGFCM [24], sFCM [26], ASIFC [25], PFCM [44] methods.

4.1   Results obtained on BrainWeb Dataset

The BrainWeb simulated T1-weighted and T2-weighted MR images of human brain are obtained from the McConnell Brain Imaging Center of the Montreal Neurological Institute, McGill University [40]. Ten different combinations of both simulated T1-weighted and T2-weighted data volumes have been gathered from which test has been carried out on volumes of 51 (image slice 50 − 100) and 81 (image slice 50 − 130) out of the total volume of 180. All of the image volumes the resolution is $181 \times 217 \times 181$ and the size is $1mm \times 1mm \times 1mm$. The image volume contains images from the following combinations respectively:

1% noise, 20% inhomogeneity	1% noise, 40% inhomogeneity
3% noise, 20% inhomogeneity	3% noise, 40% inhomogeneity
5% noise, 20% inhomogeneity	5% noise, 40% inhomogeneity
7% noise, 20% inhomogeneity	7% noise, 40% inhomogeneity
9% noise, 20% inhomogeneity	9% noise, 40% inhomogeneity

4.1.1   T1-weighted image volume

First, we present the comparative analysis on all of the above volumes in Figure 4.1 and Figure 4.2 considering cubic neighborhood of $3 \times 3 \times 3$, $5 \times 5 \times 5$, $7 \times 7 \times 7$ and $9 \times 9 \times 9$ with fuzziness of 1.25, 1.5, 1.75, 2.0, 2.25, 2.5, 2.75 and 3.0; from which we will be focusing on our best results for further comparison with previous methods.

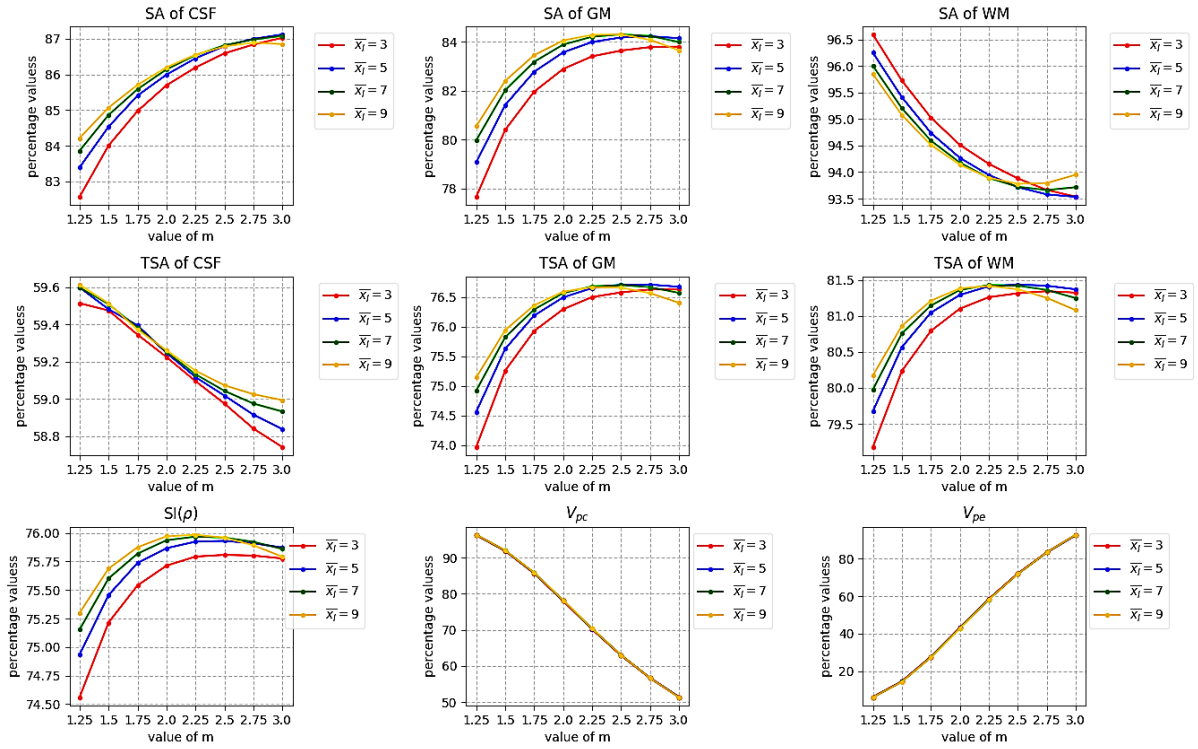*Figure 4.1: Plots of all quantitative metrics for BrainWeb T1-weighted 51 image volume having 9% noise and 40% inhomogeneity*
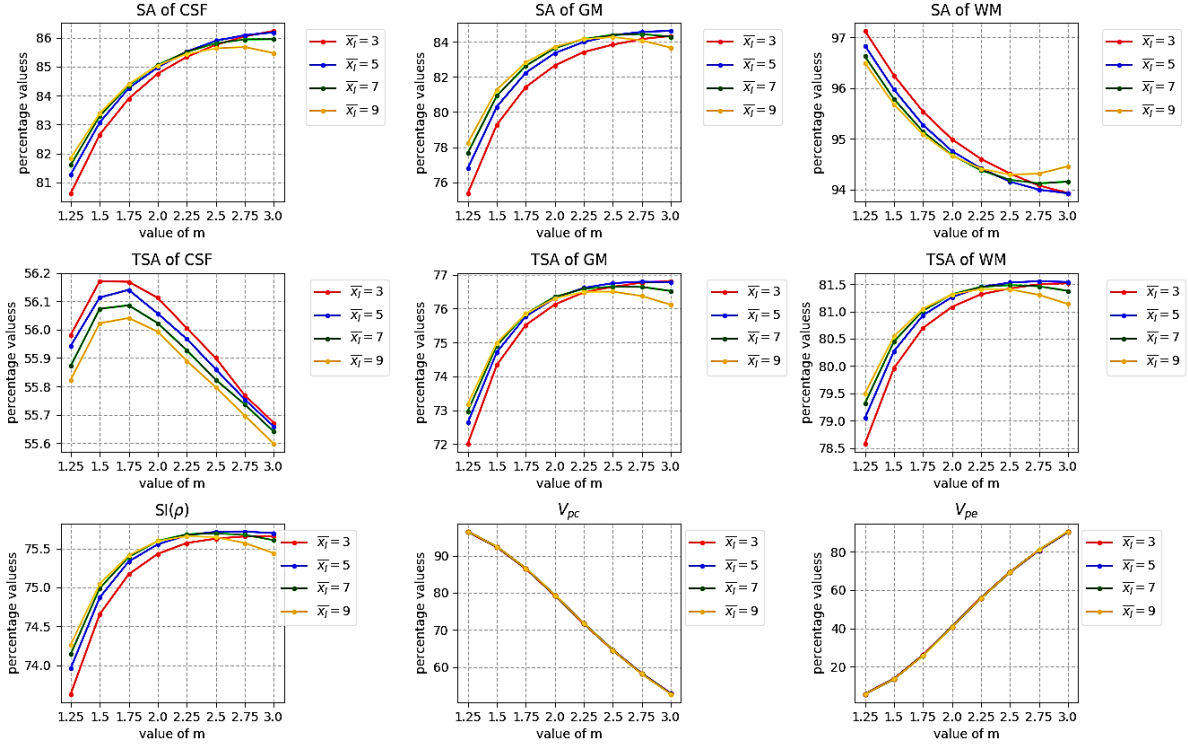
Figure 4.2: Plots of all quantitative metrics for BrainWeb T1-weighted 81 image volume having 9% noise and 40% inhomogeneity

Based on the above two Figures 4.1 and 4.2 we can come to the conclusion that for cubic neighborhood **7 × 7 × 7** and fuzziness value 1.75 the best possible results can be observed. Hence, we fix these values for the rest of the experiment and proceed forward with the qualitative results in Figure 4.3 and Figure 4.4 and quantitative metrics in Table 4.1 and Table 4.2.

In Figure 4.3 the figures (a) to (e) shows the qualitative segmentation results of the original image, segmented image, CSF segmented image, GM segmented image, WM segmented image (from left to right) respectively, by the proposed method on slice 92 of T1-weighted MR image volume having 9% noise, 40% inhomogeneity. In Figure 4.4 the figures (a) to (e) shows the qualitative segmentation results of the original 3D image, segmented 3D image, CSF segmented 3D image, GM segmented 3D image, WM 3D segmented image (from left to right) respectively, by the proposed method on T1-weighted MR image volume having 1% noise, 20% inhomogeneity.

(a)

(b)   *(c)*   *(d)*   *(e)*

Figure 4.3: (a) to (e) shows the qualitative segmentation results of the original, segmented, CSF, GM, WM images (from left to right) by the proposed method on T1-weighted MR image volume slice 92 with 9% noise, 40% inhomogeneity

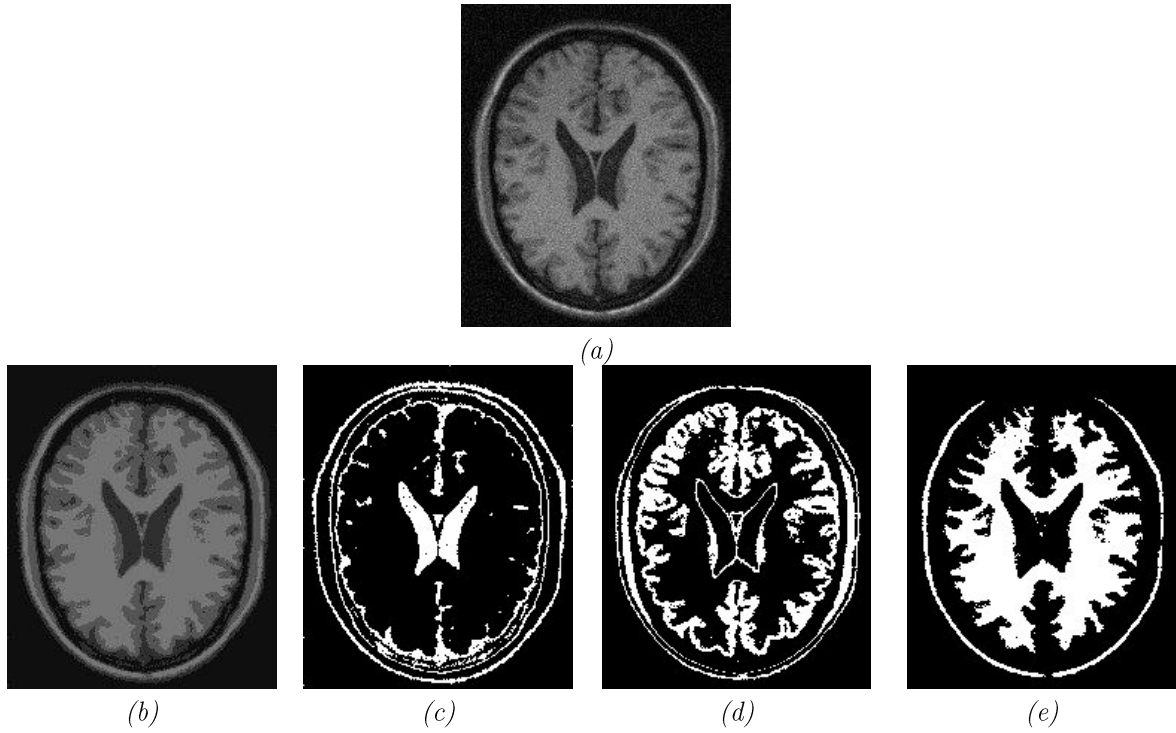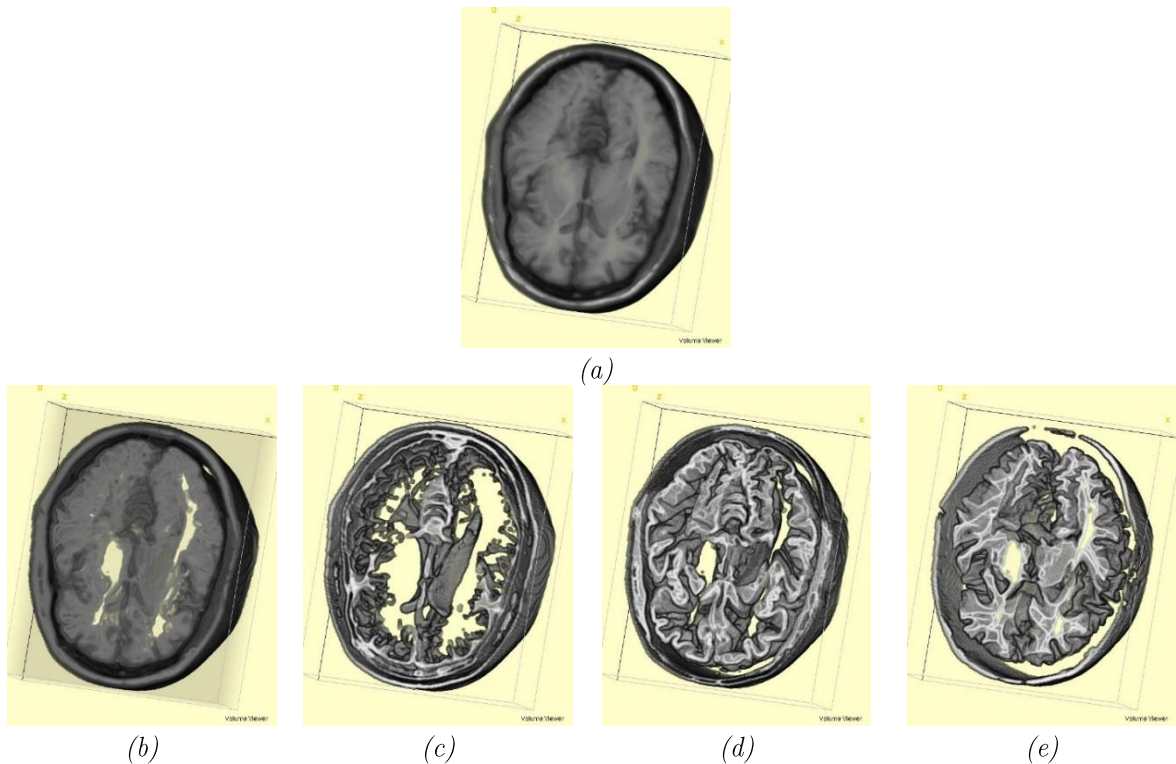*(a)*

(b)   *(c)*   *(d)*   *(e)*

Figure 4.4: (a) to (e) shows the qualitative segmentation results of the original, segmented, CSF, GM, WM 3D images (from left to right) by the proposed method on T1-weighted MR image volume with 9% noise, 40% inhomogeneity

In the following Table 4.1 we have presented a comparative study with the values of Segmentation Accuracy (*SA*) for earlier methods along with our own proposed method. As we can see our method performs better and is more stable with increasing noise and inhomogeneity.

Table 4.1: Comparative study of Segmentation Accuracy (SA) for all T1-weighted image volumes

Volumes (Noise% - IIH%)	Regions	Segmentation Accuracy (*SA*)					
		FCM	FGFCM	sFCM	ASIFC	PFCM	Proposed Method
$1-20$	CSF	0.956	0.938	0.966	0.969	0.961	0.899
	GM	0.922	0.895	0.938	0.942	0.935	0.885
	WM	0.966	0.977	0.975	0.978	0.976	0.988
$1-40$	CSF	0.938	0.917	0.944	0.947	0.950	0.896
	GM	0.874	0.853	0.931	0.934	0.875	0.866
	WM	0.918	0.959	0.968	0.973	0.940	0.969
$3-20$	CSF	0.930	0.906	0.938	0.942	0.949	0.901
	GM	0.865	0.848	0.927	0.939	0.907	0.882
	WM	0.907	0.951	0.956	0.960	0.974	0.986
$3-40$	CSF	0.910	0.893	0.921	0.926	0.925	0.896
	GM	0.849	0.835	0.922	0.924	0.850	0.863
	WM	0.898	0.944	0.947	0.952	0.937	0.966
$5-20$	CSF	0.881	0.861	0.907	0.911	0.907	0.896
	GM	0.834	0.828	0.916	0.919	0.879	0.874
	WM	0.848	0.941	0.938	0.946	0.959	0.982
$5-40$	CSF	0.837	0.832	0.861	0.867	0.875	0.890
	GM	0.825	0.821	0.909	0.911	0.837	0.856
	WM	0.840	0.916	0.926	0.933	0.925	0.962
$7-20$	CSF	0.819	0.816	0.852	0.859	0.836	0.884
	GM	0.818	0.801	0.902	0.907	0.815	0.862
	WM	0.829	0.909	0.912	0.918	0.949	0.976
$7-40$	CSF	0.807	0.795	0.849	0.852	0.817	0.879
	GM	0.782	0.792	0.895	0.989	0.772	0.845
	WM	0.795	0.906	0.903	0.908	0.926	0.956
$9-20$	CSF	0.753	0.739	0.827	0.836	0.777	0.859
	GM	0.755	0.736	0.871	0.875	0.762	0.847
	WM	0.781	0.873	0.897	0.901	0.932	0.966
$9-40$	CSF	0.742	0.731	0.824	0.829	0.753	0.856
	GM	0.742	0.725	0.862	0.868	0.737	0.832
	WM	0.765	0.876	0.873	0.880	0.914	0.946

Next in Table 4.2 a comparative study with the values of Tissue Segmentation Accuracy (*TSA*) for earlier methods and our own proposed method is presented. As we can see our method performs better and is more stable with increasing noise and inhomogeneity.

Table 4.2: Comparative study of Tissue Segmentation Accuracy (TSA) for all T1-weighted image volumes

Volumes (Noise% - IIH%)	Regions	Tissue Segmentation Accuracy (*TSA*)					
		FCM	FGFCM	sFCM	ASIFC	PFCM	Proposed Method
1 − 20	CSF	0.463	0.465	0.652	0.668	0.452	0.598
	GM	0.724	0.720	0.845	0.862	0.720	0.798
	WM	0.741	0.738	0.853	0.873	0.741	0.841
1 − 40	CSF	0.458	0.462	0.645	0.657	0.427	0.594
	GM	0.719	0.715	0.837	0.848	0.691	0.780
	WM	0.738	0.731	0.851	0.862	0.729	0.828
3 − 20	CSF	0.451	0.458	0.633	0.642	0.451	0.607
	GM	0.717	0.711	0.831	0.843	0.710	0.798
	WM	0.735	0.731	0.847	0.858	0.730	0.840
3 − 40	CSF	0.442	0.447	0.623	0.639	0.424	0.602
	GM	0.698	0.691	0.825	0.836	0.684	0.780
	WM	0.724	0.719	0.842	0.854	0.720	0.827
5 − 20	CSF	0.439	0.442	0.615	0.623	0.494	0.610
	GM	0.693	0.689	0.817	0.829	0.690	0.794
	WM	0.716	0.714	0.839	0.846	0.717	0.836
5 − 40	CSF	0.419	0.426	0.609	0.618	0.414	0.605
	GM	0.678	0.673	0.811	0.825	0.672	0.777
	WM	0.714	0.712	0.831	0.842	0.711	0.824
7 − 20	CSF	0.417	0.421	0.602	0.611	0.418	0.609
	GM	0.660	0.654	0.795	0.816	0.651	0.787
	WM	0.694	0.691	0.822	0.835	0.690	0.830
7 − 40	CSF	0.390	0.392	0.592	0.601	0.397	0.604
	GM	0.645	0.637	0.778	0.792	0.629	0.771
	WM	0.693	0.689	0.815	0.829	0.684	0.819
9 − 20	CSF	0.377	0.381	0.558	0.579	0.366	0.599
	GM	0.621	0.613	0.762	0.786	0.605	0.778
	WM	0.666	0.664	0.808	0.824	0.660	0.822
9 − 40	CSF	0.361	0.372	0.552	0.571	0.358	0.594
	GM	0.610	0.605	0.751	0.769	0.590	0.763
	WM	0.671	0.670	0.792	0.817	0.662	0.811

Based on the experiments the plots for all the quantitative metrics obtained using our proposed method for all 10 T1-weighted image volumes is shown in Figure 4.5.
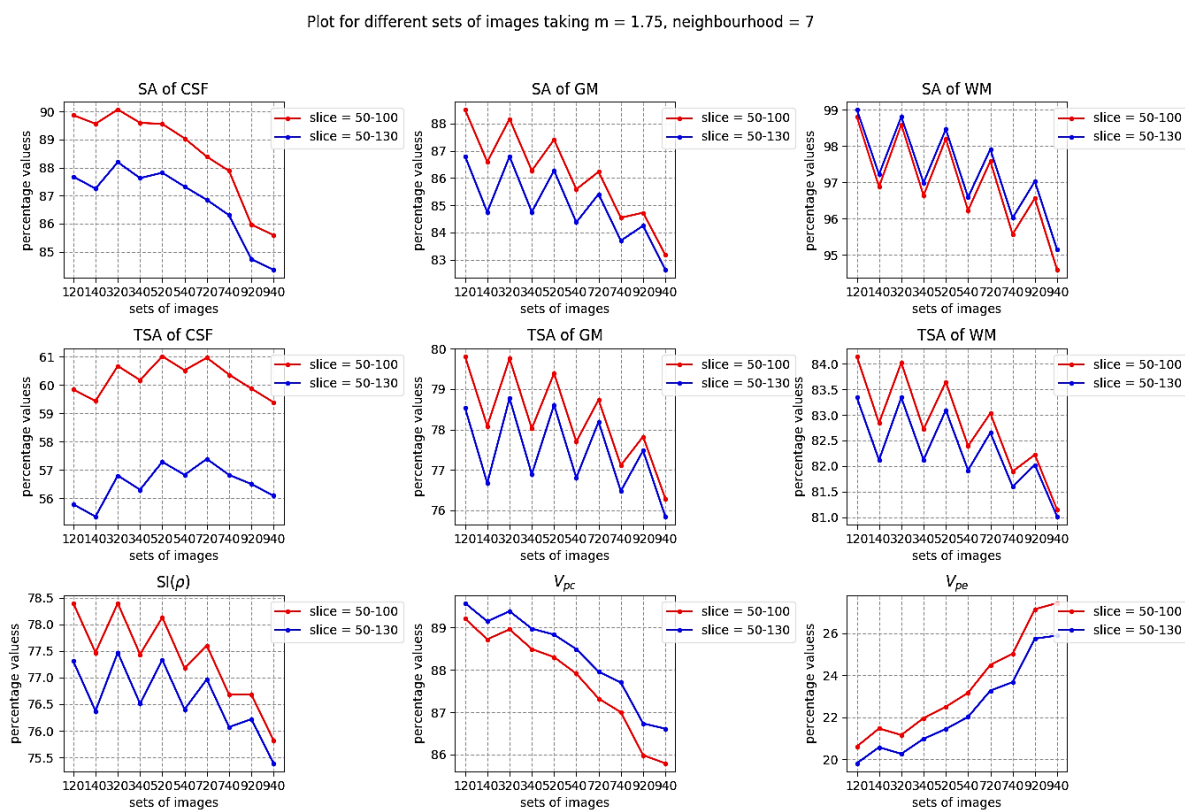

Figure 4.5: Plots of all quantitative metrics for all BrainWeb T1-weighted image volumes

4.1.2   T2-weighted image volume

Here, we have shown the comparative analysis on all of the earlier mentioned volumes in Figure 4.6 and Figure 4.7 considering cubic neighborhood of $3 \times 3 \times 3$, $5 \times 5 \times 5$, and $7 \times 7 \times 7$ with fuzziness of 1.25, 1.5, 1.75, 2.0, 2.25, 2.5, 2.75 and 3.0; from which we will be focusing on our best results for further comparison with previous methods.
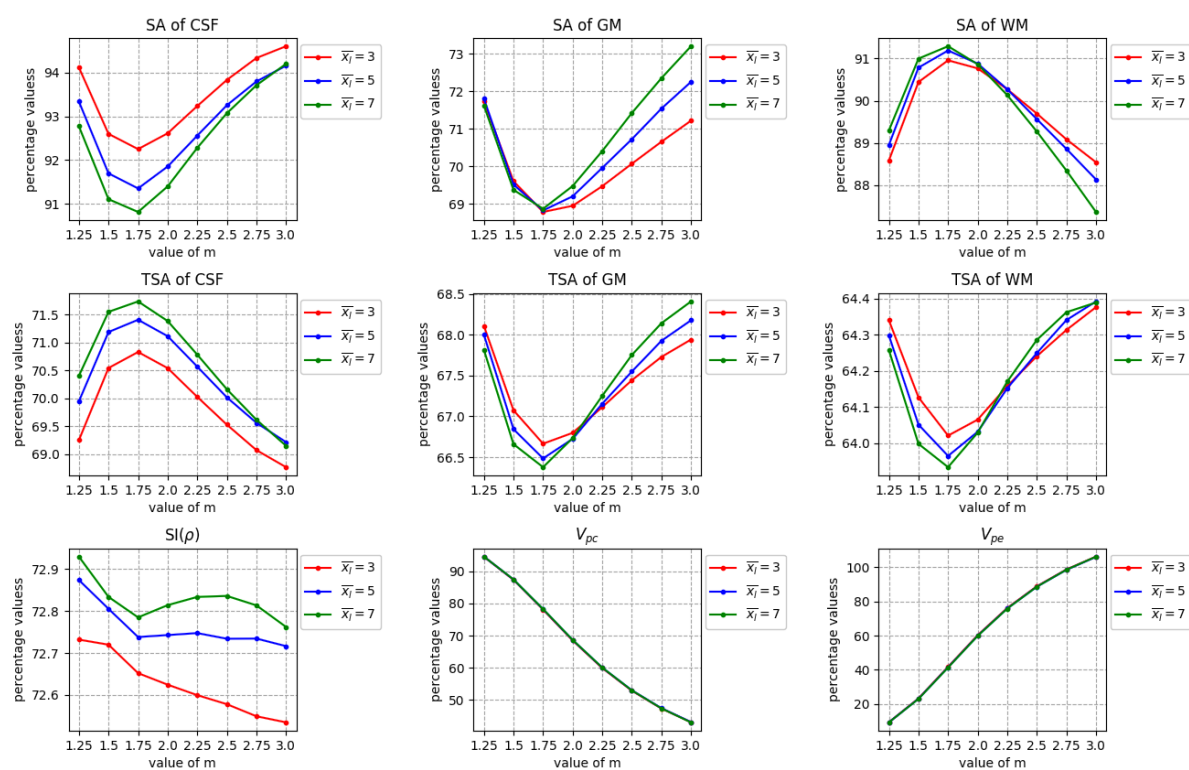

Figure 4.6: Plots of all quantitative metrics for BrainWeb T2-weighted 51 image volume having 9% noise and 40% inhomogeneity

Plot for different values of m for image 940, neighbourhood = (3, 5, 7), considering slice = 50-130
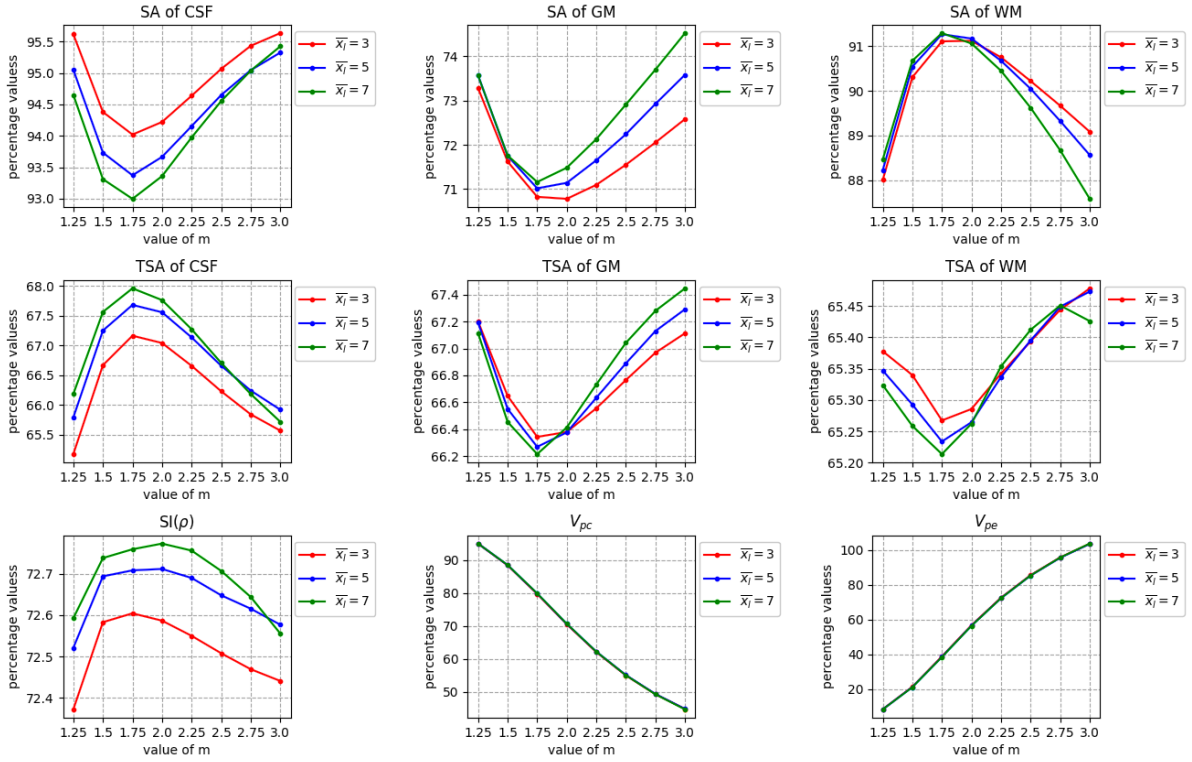
Figure 4.7: Plots of all quantitative metrics for BrainWeb T2-weighted 81 image volume having 9% noise and 40% inhomogeneity

Based on the above two Figures 4.6 and 4.7 we can come to the conclusion that for cubic neighborhood $5 \times 5 \times 5$ and fuzziness value 1.5 the best possible results can be observed. Hence, we fix these values for the rest of the experiment and proceed forward with the qualitative results in Figure 4.8 and Figure 4.9 and quantitative metrics in Table 4.3.

In Figure 4.8 the figures (a) to (e) shows the qualitative segmentation results of the original image, segmented image, CSF segmented image, GM segmented image, WM segmented image (from left to right) respectively, by the proposed method on slice 92 of T2-weighted MR image volume having 9% noise, 40% inhomogeneity. In Figure 4.9 the figures (a) to (e) shows the qualitative segmentation results of the original 3D image, segmented 3D image, CSF segmented 3D image, GM segmented 3D image, WM 3D segmented image (from left to right) respectively, by the proposed method on T2-weighted MR image volume having 1% noise, 20% inhomogeneity.
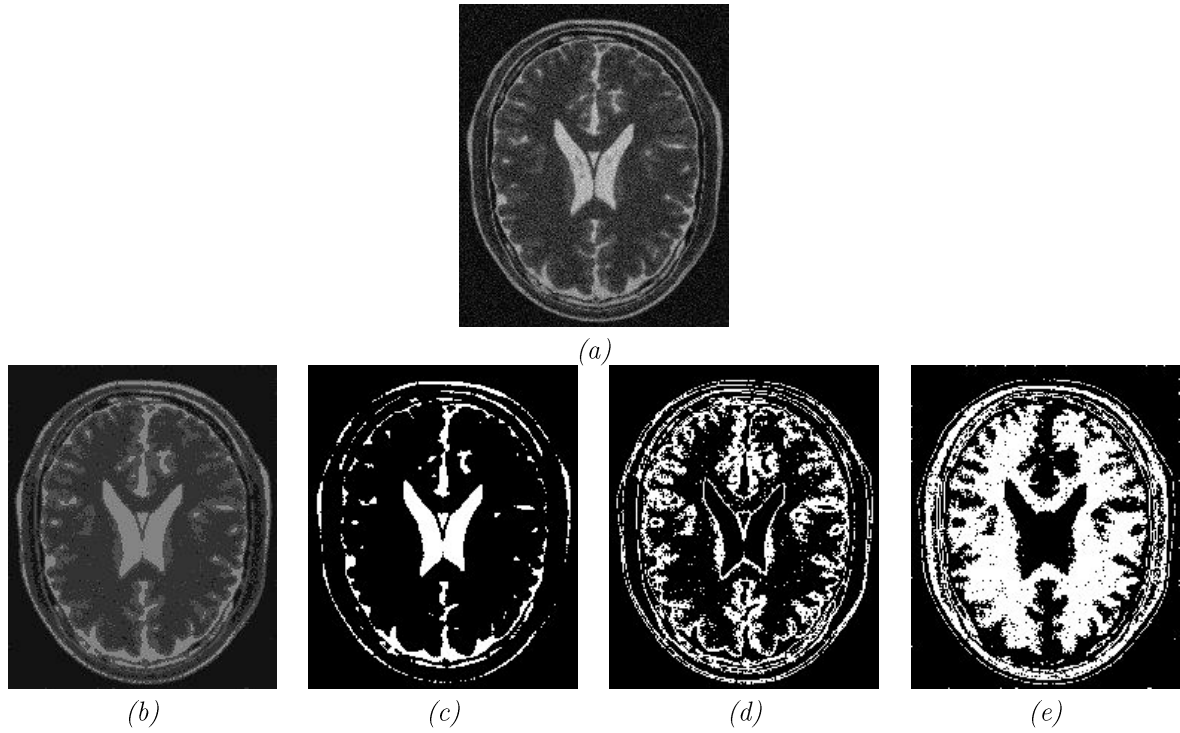
Figure 4.8: (a) to (e) shows the qualitative segmentation results of the original, segmented, CSF, GM, WM images (from left to right) by the proposed method on T2-weighted MR image volume slice 92 with 9% noise, 40% inhomogeneity
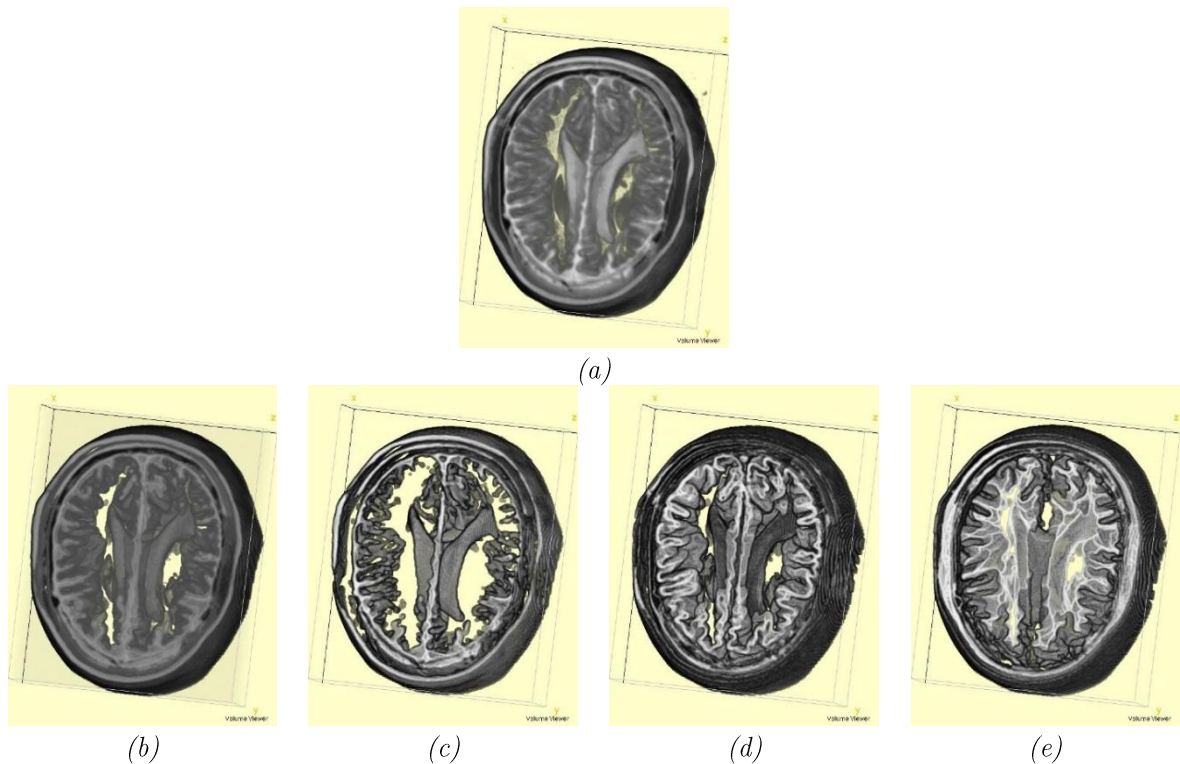

Figure 4.9: (a) to (e) shows the qualitative segmentation results of the original, segmented, CSF, GM, WM images (from left to right) by the proposed method on T2-weighted MR image volume with 1% noise, 20% inhomogeneity

In Table 4.3 the values of Segmentation Accuracy (*SA*) and Tissue Segmentation Accuracy (*TSA*) for our proposed method is shown. We can see our method is stable with increasing noise and inhomogeneity.

Table 4.3: Results of Segmentation Accuracy (SA) and Tissue Segmentation Accuracy (TSA) for all T2-weighted image volumes

Volumes (Noise% - IIH%)	Regions	Segmentation Accuracy (*SA*) of proposed method	Tissue Segmentation Accuracy (*TSA*) of proposed method
1 – 20	CSF	0.971	0.684
	GM	0.863	0.794
	WM	0.972	0.709
1 – 40	CSF	0.959	0.701
	GM	0.847	0.778
	WM	0.953	0.693
3 – 20	CSF	0.967	0.686
	GM	0.837	0.778
	WM	0.968	0.706
3 – 40	CSF	0.954	0.704
	GM	0.821	0.762
	WM	0.953	0.691
5 – 20	CSF	0.960	0.689
	GM	0.799	0.752
	WM	0.958	0.693
5 – 40	CSF	0.945	0.707
	GM	0.783	0.736
	WM	0.947	0.679
7 – 20	CSF	0.949	0.692
	GM	0.754	0.718
	WM	0.944	0.675
7 – 40	CSF	0.933	0.711
	GM	0.741	0.705
	WM	0.935	0.664
9 – 20	CSF	0.937	0.693
	GM	0.709	0.681
	WM	0.915	0.650
9 – 40	CSF	0.917	0.712
	GM	0.695	0.668
	WM	0.908	0.640

Based on the experiments the plots for all the quantitative metrics obtained using our proposed method for all 10 T2-weighted image volumes is shown in Figure 4.10
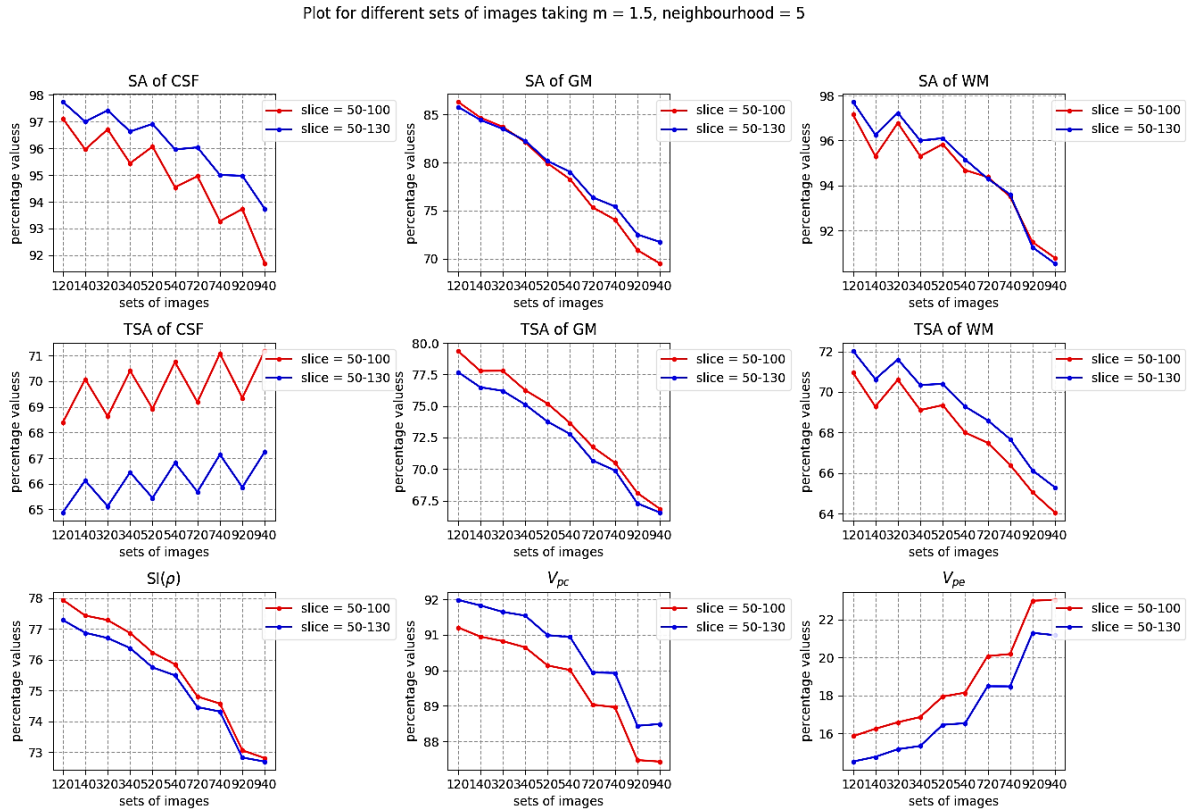

Figure 4.10: Plots of all quantitative metrics for all BrainWeb T2-weighted image volumes

4.2 Results obtained on IBSR dataset

IBSR was originally supported by the NIH from the National Institute of Neurological Disorders and Stroke (NINDS). This grant funds research in MR brain segmentation by researchers at Boston University, Draper Laboratory, Northeastern University, Massachusetts Institute of Technology, and Massachusetts General Hospital / Harvard Medical School. Since the original web site is no longer fully functional, all data has been transferred and hosted at NITRC. However, for this experiment we have used the earlier data that has been collected.

The test has been carried out on volumes of 30 (image slice 123 − 152) and 40 (image slice 115 − 154) [only for final analysis in Figure 4.14] out of the total volume of 256.

All of the image volumes the resolution is $128 \times 256 \times 256$. There are 14 image volumes out of which we have obtained substantial results for 3 image volumes (1, 3, 5).

First, we present the comparative analysis on all the three volumes in Figure 4.11 considering neighborhood of 3, 5 and 7 with fuzziness of 1.25, 1.5, 1.75, 2.0, 2.25, 2.5, 2.75, 3.0 and 3.25; from this we will be focusing on our best results for further comparison with previous methods.
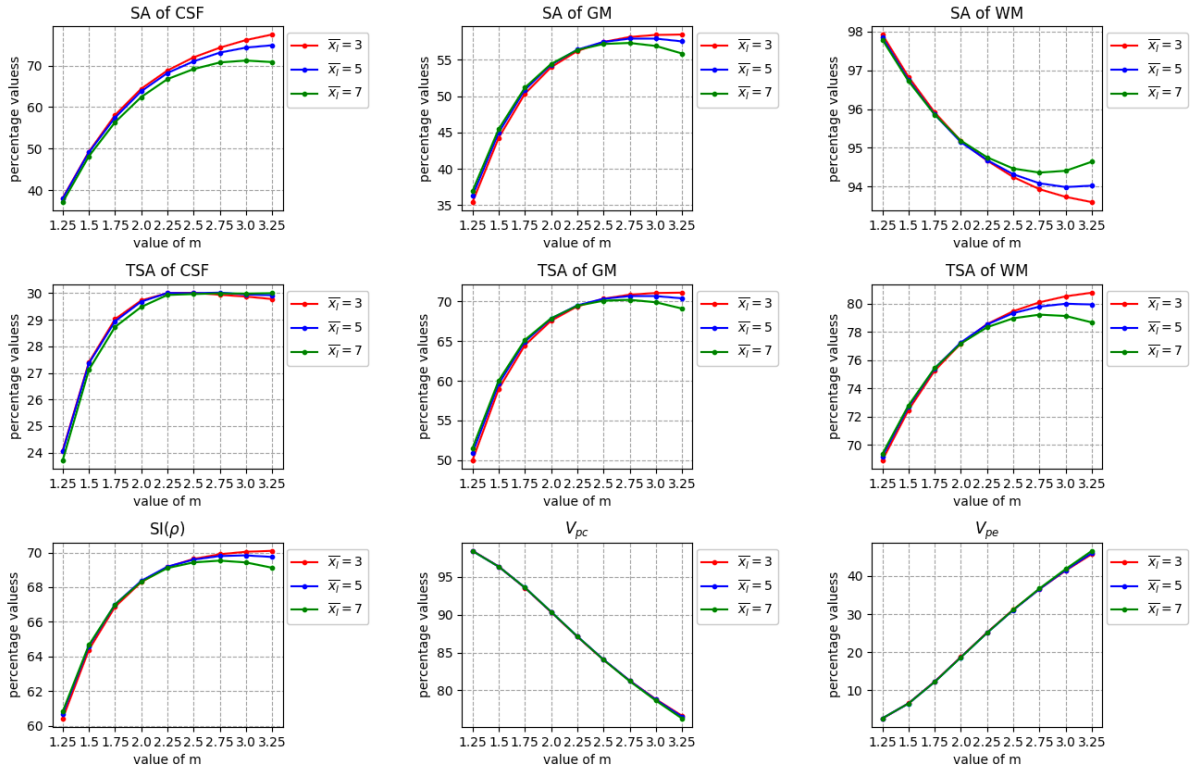

Figure 4.11: Plots of all quantitative metrics for IBSR image volume-1 considering 30 image slice as volume

Based on the above Figure 4.11 we can come to the conclusion that for neighborhood 5 and fuzziness value 2.5 the best possible results can be observed. Hence, we fix these values for the rest of the experiment and proceed with the qualitative results in Figure 4.12 and Figure 4.13 followed by quantitative metrics in Table 4.4 and Table 4.5.

In Figure 4.1 the figures (a) to (e) shows the qualitative segmentation results of the original image, segmented image, CSF segmented image, GM segmented image, WM segmented image (from left to right) respectively, by the proposed method on slice 140 of IBSR image volume 1. In Figure 4.2 the figures (a) to (e) shows the qualitative

segmentation results of the original 3D image, segmented 3D image, CSF segmented 3D image, GM segmented 3D image, WM 3D segmented image (from left to right) respectively, by the proposed method on IBSR image volume 1.

(a)

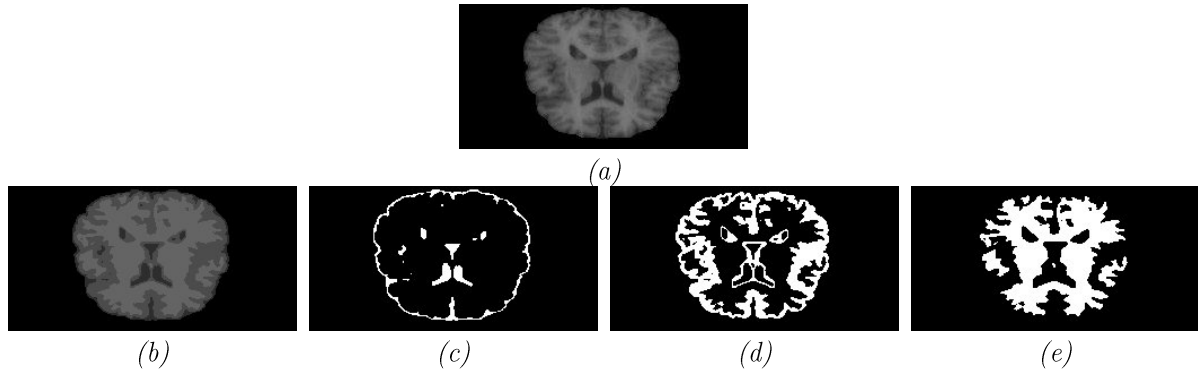

(b)   *(c)*   *(d)*   *(e)*

Figure 4.12: (a) to (e) shows the qualitative segmentation results of the original, segmented, CSF, GM, WM images (from left to right) by the proposed method on volume-1 of IBSR dataset, slice 140
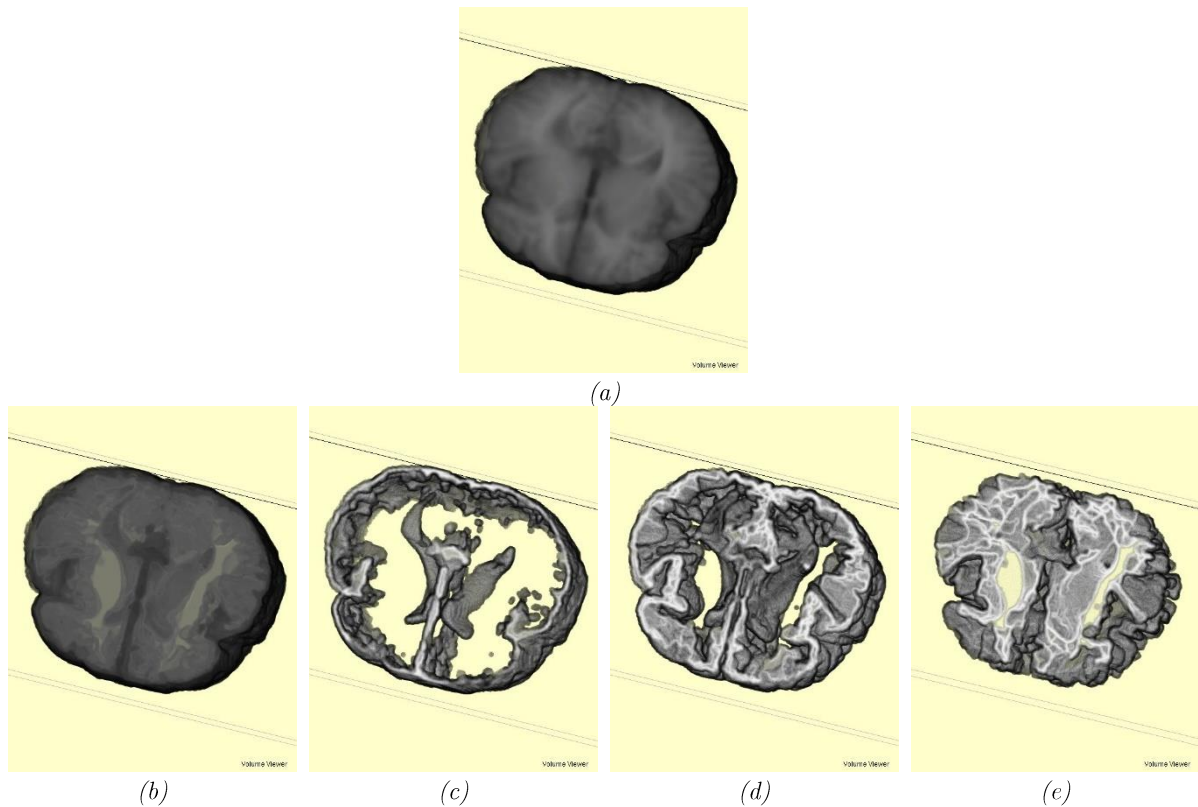

(a)

(b)   *(c)*   *(d)*   *(e)*

Figure 4.13: (a) to (e) shows the qualitative segmentation results of the original, segmented, CSF, GM, WM images (from left to right) by the proposed method on volume-1 of IBSR dataset

In the following Table 4.4 we have presented a comparative study with the values of Segmentation Accuracy (*SA*) for earlier methods along with our own proposed method for the specified volumes. We can see our method performs in close proximity or in some cases better in identifying WM specifically.

Table 4.4: Comparative study of Segmentation Accuracy (SA) for IBSR image volumes

Volumes (Noise% - IIH%)	Regions	Segmentation Accuracy (*SA*)					
		FCM	FGFCM	sFCM	ASIFC	PFCM	Proposed Method
Volume 1	CSF	0.767	0.752	0.832	0.837	0.726	0.710
	GM	0.629	0.613	0.693	0.696	0.620	0.577
	WM	0.950	0.948	0.947	0.958	0.955	0.943
Volume 2	CSF	0.756	0.745	0.778	0.782	0.737	0.542
	GM	0.748	0.729	0.786	0.793	0.732	0.619
	WM	0.944	0.951	0.949	0.956	0.954	0.957
Volume 5	CSF	0.623	0.611	0.631	0.636	0.611	0.478
	GM	0.753	0.749	0.827	0.831	0.799	0.631
	WM	0.632	0.758	0.753	0.778	0.775	0.964

Next in Table 4.5 a comparative study with the values of Tissue Segmentation Accuracy (*TSA*) for earlier methods and our own proposed method is presented. We can see our method performs in close proximity or in some cases better in identifying GM and WM specifically.

Table 4.5: Comparative study of Tissue Segmentation Accuracy (TSA) for IBSR image volumes

Volumes (Noise% - IIH%)	Regions	Tissue Segmentation Accuracy (*TSA*)					
		FCM	FGFCM	sFCM	ASIFC	PFCM	Proposed Method
Volume 1	CSF	0.534	0.537	0.601	0.620	0.633	0.299
	GM	0.622	0.619	0.412	0.738	0.608	0.703
	WM	0.664	0.657	0.476	0.779	0.650	0.793
Volume 2	CSF	0.630	0.633	0.711	0.731	0.629	0.253
	GM	0.651	0.642	0.724	0.758	0.640	0.736
	WM	0.707	0.689	0.721	0.740	0.701	0.826
Volume 5	CSF	0.528	0.538	0.543	0.562	0.569	0.245
	GM	0.646	0.632	0.710	0.731	0.733	0.742
	WM	0.621	0.618	0.653	0.689	0.681	0.818

Based on the experiments the plots for all the quantitative metrics obtained using our proposed method for the 3 IBSR image volumes is shown in Figure 4.14. It should be noted that the total average is considered for image volume of 40 (image slice 115 – 154).
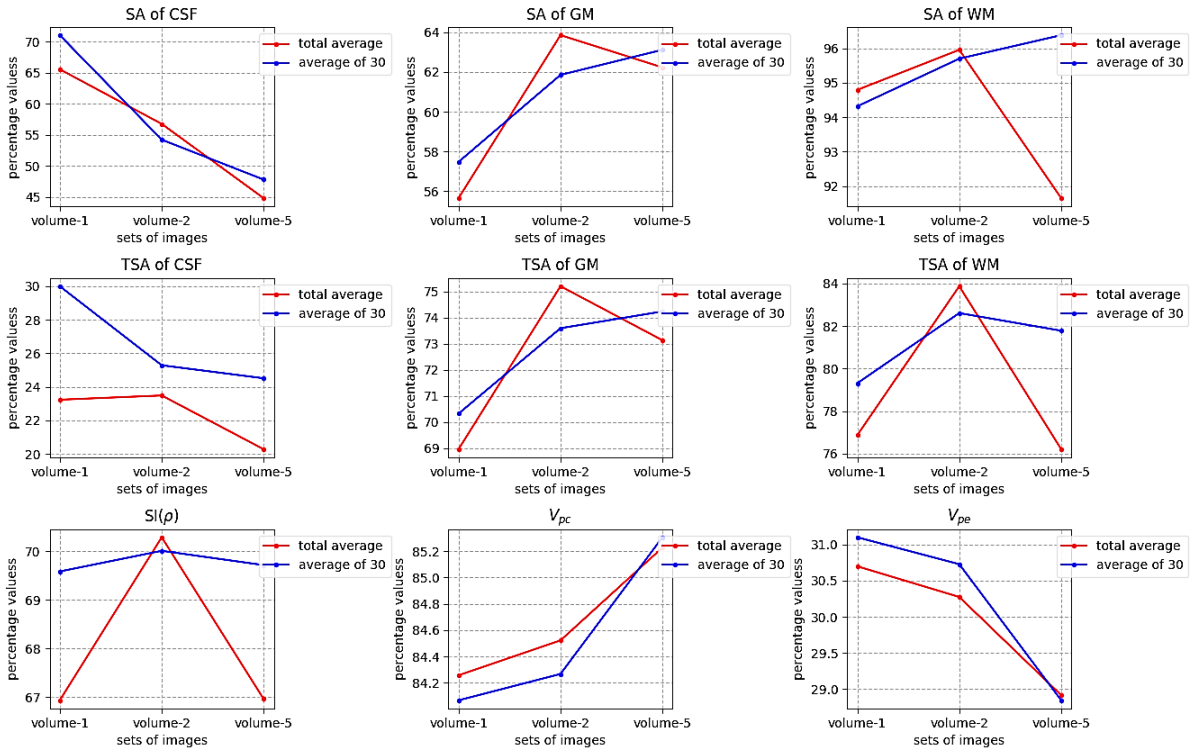
Figure 4.14: Plots of all quantitative metrics for IBSR image volume 1, 2 and 5

## 4.3 Results obtained on images of real-patient data

We have examined the performance of the proposal method on the image volumes constructed from of all real-patient MR image data which are collected from the Advanced Medical Research Institute (AMRI) Hospital, Kolkata, India and EKO X-RAY & IMAGING INSTITUTE, Kolkata, India. As the ground truth of segmentation for real-patient MRI images is not usually available, thereby the performance of the proposed method on the real-patient MR data is evaluated first qualitatively and later quantitatively in terms of cluster validity functions.

4.3.1 Real patient 1

First, we present the qualitative results of the patient 1 in 2D format in Figure 4.15 and 3D format in Figure 4.16, followed by a small analysis of how the Partition Coefficient $\left(V_{pc}\right)$ and Partition Entropy $\left(V_{pe}\right)$ varies with different values of neighborhood and fuzziness in Figure 4.17.
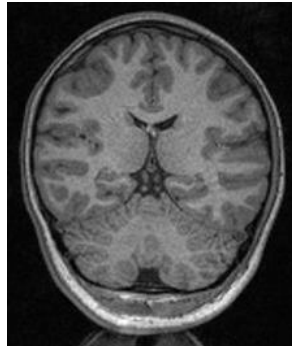
(a)
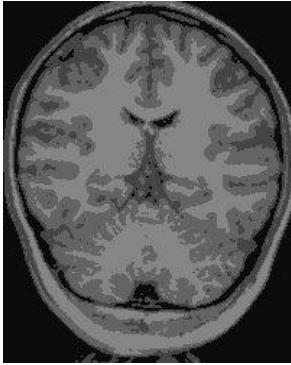
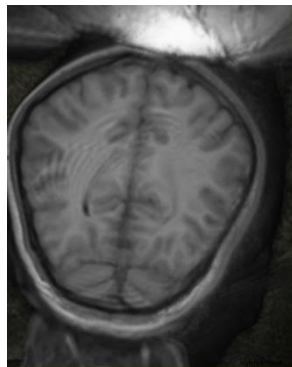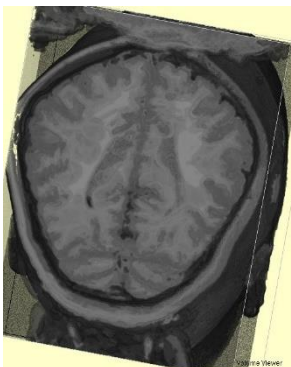*(b)*   *(c)*   *(d)*   *(e)*
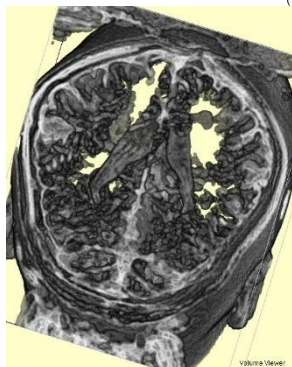
Figure 4.15: (a) to (e) shows qualitative segmentation results of the original, segmented, CSF, GM, WM images (from left to right) of real patient 1 by the proposed method
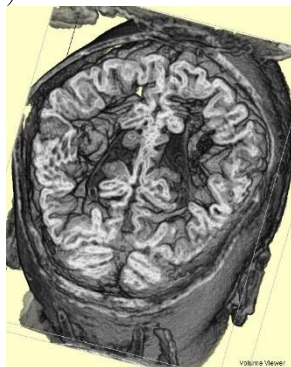

(a)

(b)   *(c)*   *(d)*   *(e)*

Figure 4.16: (a) to (e) shows qualitative segmentation results of the original, segmented, CSF, GM, WM 3D images (from left to right) of real patient 1 by the proposed method
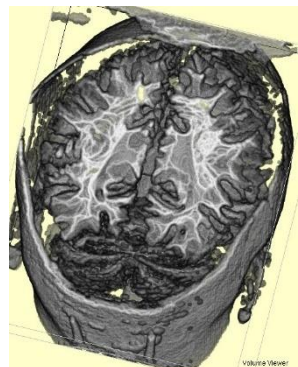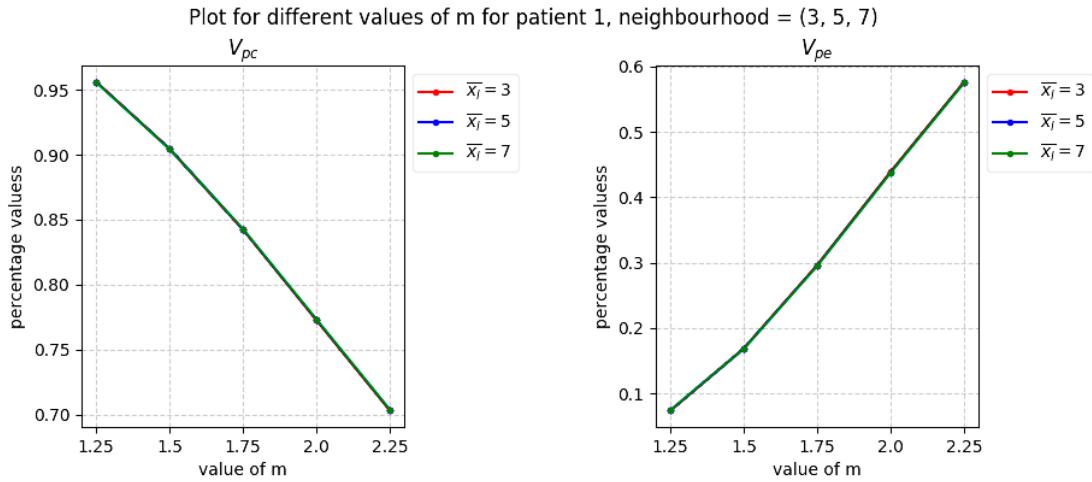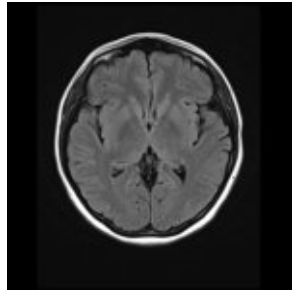
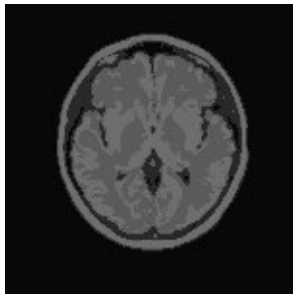*Figure 4.17: Plots for V_{pc} and V_{pe} for patient 1.*

From the qualitative analysis in Figure 4.15 and Figure 4.16 we can say that we have obtained superior results on the images of real patient 1. By observing the graphs in Figure 4.17 it can stated that algorithm that for lower values of degree of fuzziness we have reported higher result in V_{pc} and V_{pe}.

4.3.2   Real patient 2

First, we present the qualitative results of the patient 2 in 2D format in Figure 4.18 and 3D format in Figure 4.19, followed by a small analysis of how the Partition Coefficient $\left(V_{pc}\right)$ and Partition Entropy $\left(V_{pe}\right)$ varies with different values of neighborhood and fuzziness in Figure 4.20.

(a)

(b)   *(c)*   *(d)*   *(e)*

Figure 4.18: (a) to (e) shows qualitative segmentation results of the original, segmented, CSF, GM, WM images (from left to right) of real patient 2 by the proposed method
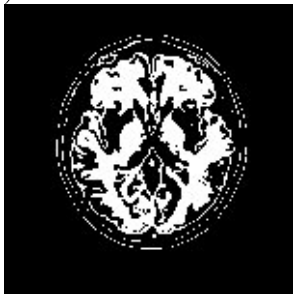

(a)

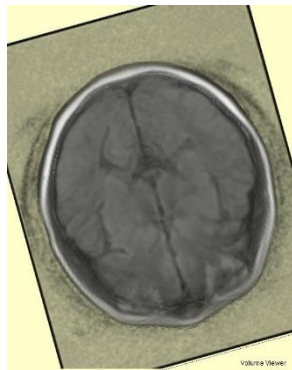*(b)*   *(c)*   *(d)*   *(e)*

Figure 4.19: (a) to (e) shows qualitative segmentation results of the original, segmented, CSF, GM, WM 3D images (from left to right) of real patient 2 by the proposed method

Figure 4.20: Plots for V_{pc} and V_{pe} for patient 2.

From the qualitative analysis in Figure 4.18 and Figure 4.19 we can say that we have obtained superior results on the images of real patient 2. By observing the graphs in Figure 4.20 it can stated that algorithm that for lower values of degree of fuzziness we have reported higher result in V_{pc} and V_{pe}.

4.3.3 Real patient 3

First, we present the qualitative results of the patient 3 in 2D format in Figure 4.21 and 3D format in Figure 4.22, followed by a small analysis of how the Partition Coefficient $\left(V_{pc}\right)$ and Partition Entropy $\left(V_{pe}\right)$ varies with different values of neighborhood and fuzziness in Figure 4.23.
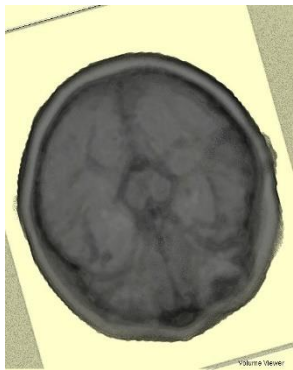

Figure 4.21: (a) to (e) shows qualitative segmentation results of the original, segmented, CSF, GM, WM images (from left to right) of real patient 3 by the proposed method
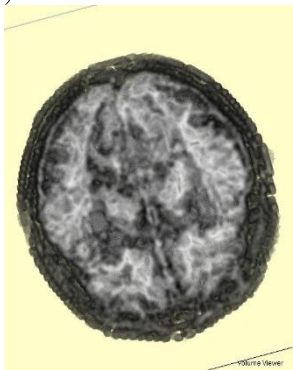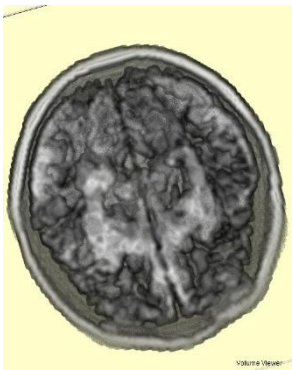
(a)

(b)   *(c)*   *(d)*   *(e)*

Figure 4.22: (a) to (e) shows qualitative segmentation results of the original, segmented, CSF, GM, WM 3D images (from left to right) of real patient 3 by the proposed method
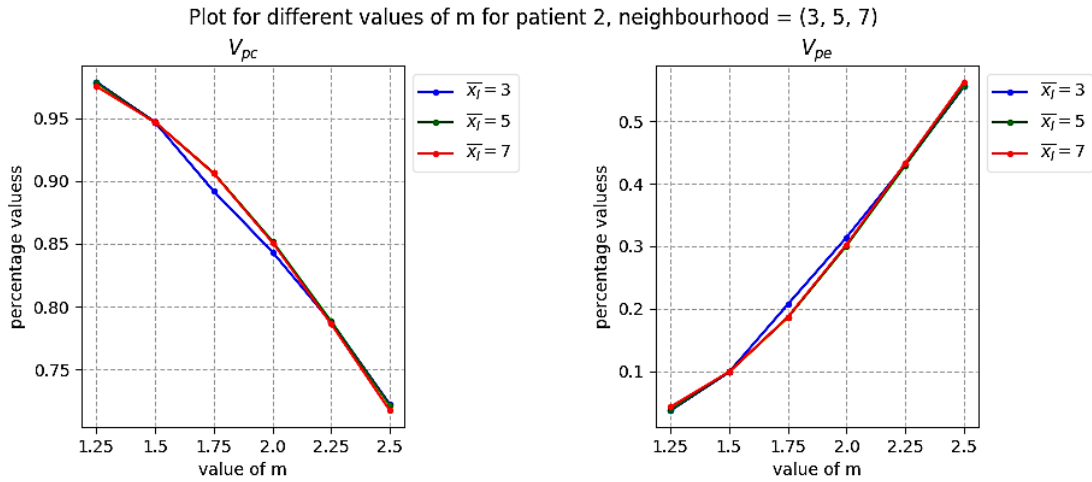

Figure 4.23: Plots for V_{pc} and V_{pe} for patient 3.

From the qualitative analysis in Figure 4.21 and Figure 4.22 we can say that we have obtained superior results on the images of real patient 3. By observing the graphs in Figure 4.23 it can stated that algorithm that for lower values of degree of fuzziness we have reported higher result in V_{pc} and V_{pe}.

4.3.4   Real patient 4

First, we present the qualitative results of the patient 4 in 2D format in Figure 4.24 and 3D format in Figure 4.25, followed by a small analysis of how the Partition Coefficient $\left(V_{pc}\right)$ and Partition Entropy $\left(V_{pe}\right)$ varies with different values of neighborhood and fuzziness in Figure 4.26.

(a)

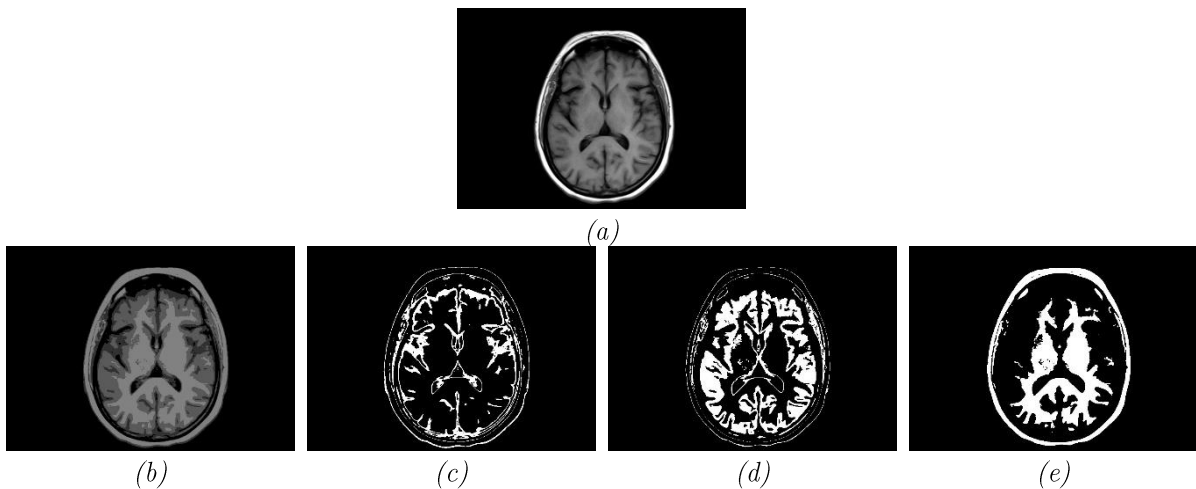(b)   (c)   (d)   (e)
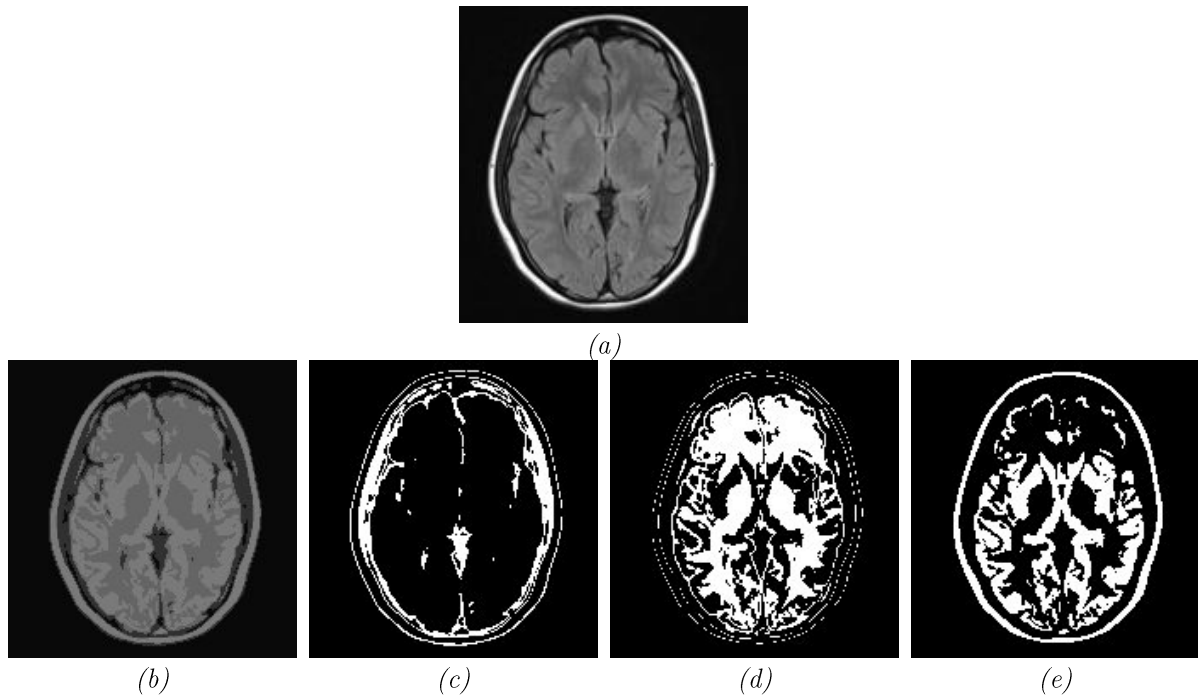
Figure 4.24: (a) to (e) shows qualitative segmentation results of the original, segmented, CSF, GM, WM images (from left to right) of real patient 4 by the proposed method

(a)

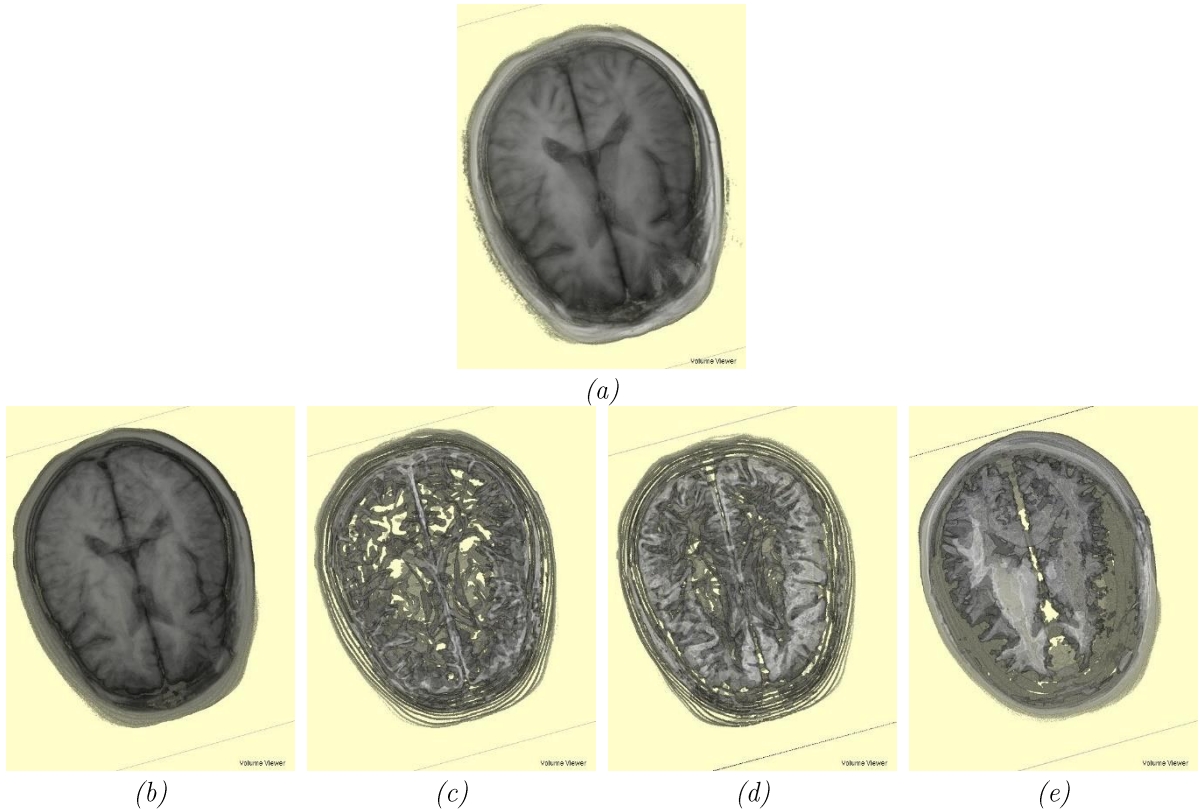*(b)*   *(c)*   *(d)*   *(e)*
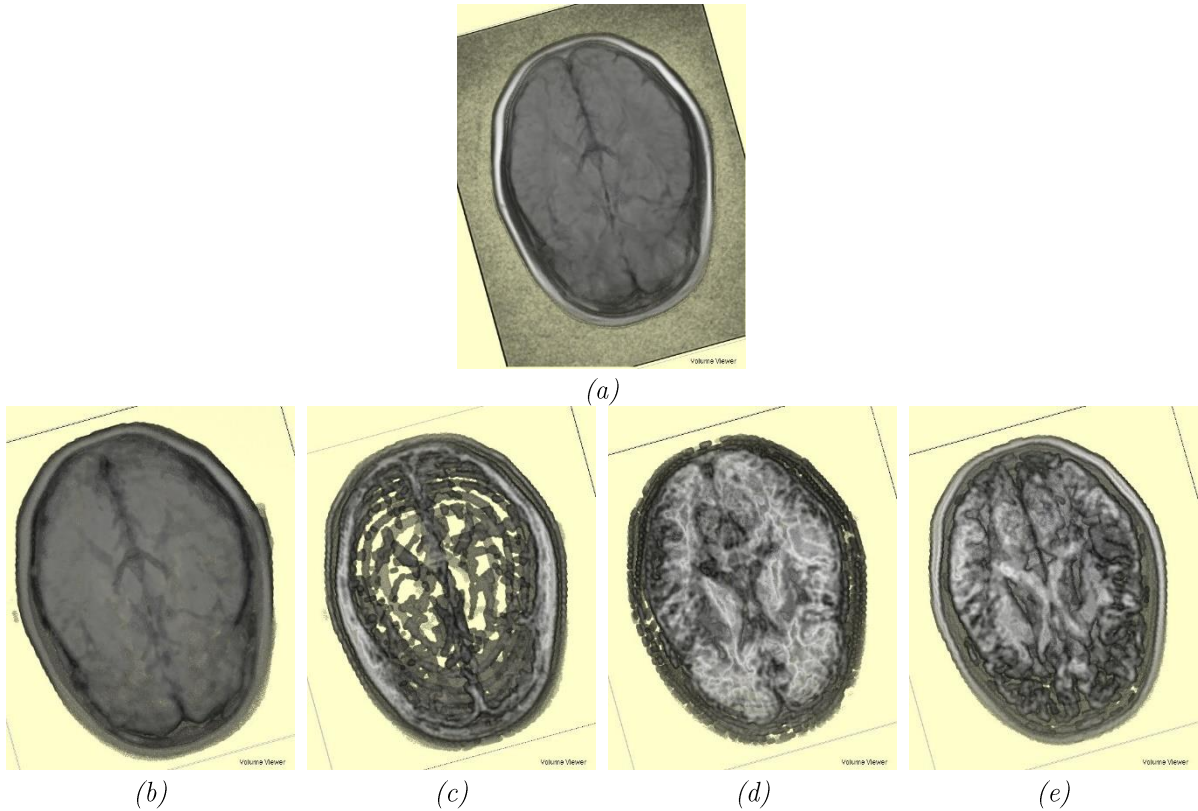
Figure 4.25: (a) to (e) shows qualitative segmentation results of the original, segmented, CSF, GM, WM 3D images (from left to right) of real patient 4 by the proposed method
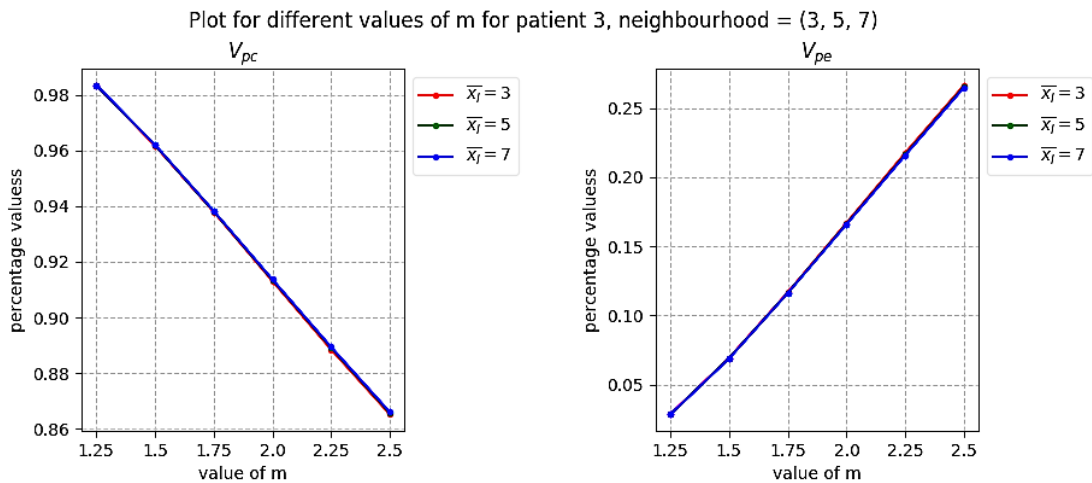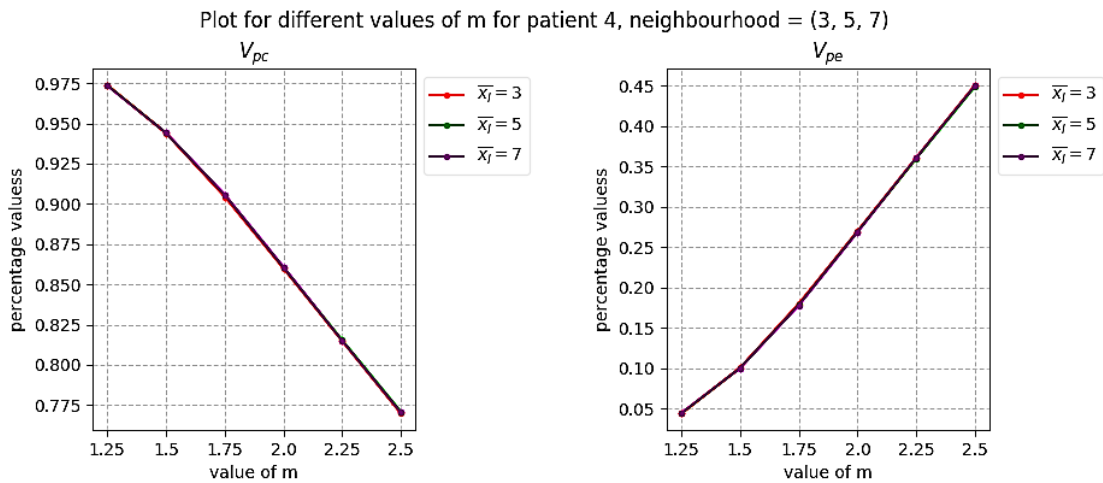

Figure 4.26: Plots for V_{pc} and V_{pe} for patient 4.

From the qualitative analysis in Figure 4.24 and Figure 4.25 we can say that we have obtained superior results on the images of real patient 4. By observing the graphs in Figure 4.26 it can stated that algorithm that for lower values of degree of fuzziness we have reported higher result in V_{pc} and V_{pe}.

A final comparison of the Partition Coefficient (V_{pc}) and Partition Entropy (V_{pe}) between previous methods and our own methods is shown in the following Table 4.6. The best results that can be observed from the graphs 4.17, 4.20, 4.23 and 4.26 is taken into consideration and recorded in the table below.

We can observe that our proposed method gives superior results for all the test cases on real patient images across the board.

Table 4.6: Comparative study of V_{pc} and V_{pe} for all real patient images

| Volume	Method	V_{pc}	V_{pe}
Real patient 1 (Male)	FCM	0.705	0.558
	FGFCM	0.815	0.329
	sFCM	0.886	0.294
	ASIFC	0.911	0.206
	PFCM	0.924	0.137
	Proposed Method	0.956	0.074
Real patient 2 (Female)	FCM	0.791	0.253
	FGFCM	0.811	0.159
	sFCM	0.835	0.074
	ASIFC	0.897	0.053
	PFCM	0.905	0.087
	Proposed Method	0.978	0.038
Real patient 3 (Female)	FCM	0.741	0.507
	FGFCM	0.852	0.287
	sFCM	0.883	0.228
	ASIFC	0.912	0.196
	PFCM	0.921	0.129
	Proposed Method	0.983	0.028
Real patient 4 (Female)	FCM	0.870	0.273
	FGFCM	0.893	0.193
	sFCM	0.907	0.178
	ASIFC	0.922	0.143
	PFCM	0.935	0.112
	Proposed Method	0.974	0.044

Chapter 5:

Conclusion and Future Scope

In this thesis entitled "Volumetric Brain MR Image Segmentation using Entropy based Fuzzy Clustering Algorithm" an image segmentation method has been presented involving Shannon entropy to improve the robustness to the noise and intensity inhomogeneity. This proposed method has been examined extensively both in qualitative and quantitative manner and has been compared with previous algorithms. From the experimental results it is clear that with proper parameters of neighborhood and fuzziness the results are definitely better. Also, the proposed method is tolerant to noise and intensity inhomogeneity and thereby can produce superior results irrespective of the aforementioned hurdle.

Chapter 6:

References

[1] Linda G. Shapiro and George C. Stockman. *Computer Vision*, pages 305–307. Prentice Hall, 2011.

[2] Yong Yang. Image segmentation based on fuzzy clustering with neighborhood information. *Optica Applicata*, 39(1), 2009.

[3] Jannis Heil, Volker Häring, Bernd Marschner, and Britta Stumpe. Advantages of fuzzy k-means over k-means clustering in the classification of diffuse reflectance soil spectra: A case study with west African soils. *Geoderma*, 337: 11–21, 2019.

[4] A. Ahmadvand and M. Daliri. Brain MR image segmentation methods and applications. *OMICS J Radiol*, 3(4): e130, 2014.

[5] Ivana Despotović, Bart Goossens, and Wilfried Philips. MRI segmentation of the human brain: challenges, methods, and applications. *Computational and mathematical methods in medicine*, 2015.

[6] Sudip Kumar Adhikari, Jamuna Kanta Sing, Dipak Kumar Basu, and Mita Nasipuri. Conditional spatial fuzzy c-means clustering algorithm for segmentation of MRI images. *Applied soft computing*, 34: 758–769, 2015.

[7] Mohd Ali Balafar, Abdul Rahman Ramli, M. Iqbal Saripan, and Syamsiah Mashohor. Review of brain MRI image segmentation methods. *Artificial Intelligence Review*, 33(3): 261–274, 2010.

[8] Dzung L. Pham, Chenyang Xu, and Jerry L. Prince. Current methods in medical image segmentation. *Annual review of biomedical engineering*, 2(1): 315–337, 2000.

[9] Sílvia Delgado Olabarriaga and Arnold W.M. Smeulders. Interaction in the segmentation of medical images: A survey. *Medical image analysis*, 5(2): 127–142, 2001.

[10] Li Ma and Richard C. Staunton. A modified fuzzy c-means image segmentation algorithm for use with uneven illumination patterns. *Pattern recognition*, 40(11): 3005–3011, 2007.

[11] F.B. Tek, A.G. Dempster, and I. Kale. Noise sensitivity of watershed segmentation for different connectivity: experimental study. *Electronics Letters*, 40(21): 1332–1333, 2004.

[12] James C. Bezdek. Pattern recognition with fuzzy objective function algorithms. 1981.

[13] Witold Pedrycz. Conditional fuzzy c-means. *Pattern Recognition Letters*, 17(6): 625–631, 1996.

[14] Yannis A. Tolias and Stavros M. Panas. Image segmentation by a fuzzy clustering algorithm using adaptive spatially constrained membership functions. *IEEE Transactions on Systems, Man, and Cybernetics-Part A: Systems and Humans*, 28(3): 359–369, 1998.

[15] Mohamed N. Ahmed, Sameh M. Yamany, Nevin Mohamed, Aly A. Farag, and Thomas Moriarty. A modified fuzzy c-means algorithm for bias field estimation and segmentation of MRI data. *IEEE transactions on medical imaging*, 21(3): 193–199, 2002.

[16] A.W.C. Liew, S.H. Leung, and W.H. Lau. Fuzzy image clustering incorporating spatial continuity. *IEE Proceedings-Vision, Image and Signal Processing*, 147(2): 185–192, 2000.

[17] Dzung L. Pham and Jerry L. Prince. An adaptive fuzzy c-means algorithm for image segmentation in the presence of intensity inhomogeneities. *Pattern recognition letters*, 20(1): 57–68, 1999.

[18] Alan Wee-Chung Liew and Hong Yan. An adaptive spatial fuzzy clustering algorithm for 3-D MR image segmentation. *IEEE transactions on medical imaging*, 22(9): 1063–1075, 2003.

[19] Ze-Xuan Ji, Quan-Sen Sun, and De-Shen Xia. Retracted: A framework with modified fast FCM for brain MR images segmentation, 2011.

[20] Xiang-Yang Wang and Juan Bu. A fast and robust image segmentation using fcm with spatial information. *Digital Signal Processing*, 20(4): 1173–1182, 2010.

[21] Stelios Krinidis and Vassilios Chatzis. A robust fuzzy local information c-means clustering algorithm. *IEEE transactions on image processing*, 19(5): 1328–1337, 2010.

[22] J.C. Noordam and W.H.A.M. Van Den Broek. Multivariate image segmentation based on geometrically guided fuzzy c-means clustering. *Journal of Chemometrics: A Journal of the Chemometrics Society*, 16(1): 1–11, 2002.

[23] Songcan Chen and Daoqiang Zhang. Robust image segmentation using FCM with spatial constraints based on new kernel-induced distance measure. *IEEE Transactions on Systems, Man, and Cybernetics, Part B (Cybernetics)*, 34(4): 1907–1916, 2004.

[24] Weiling Cai, Songcan Chen, and Daoqiang Zhang. Fast and robust fuzzy c-means clustering algorithms incorporating local information for image segmentation. *Pattern recognition*, 40(3): 825–838, 2007.

[25] Zhimin Wang, Qing Song, Yeng Chai Soh, and Kang Sim. An adaptive spatial information-theoretic fuzzy clustering algorithm for image segmentation. *Computer Vision and Image Understanding*, 117(10): 1412–1420, 2013.

[26] Keh-Shih Chuang, Hong-Long Tzeng, Sharon Chen, Jay Wu, and Tzong-Jer Chen. Fuzzy c-means clustering with spatial information for image segmentation. *computerized medical imaging and graphics*, 30(1): 9–15, 2006.

[27] Cunyong Qiu, Jian Xiao, Long Yu, Lu Han, and Muhammad Naveed Iqbal. A modified interval type-2 fuzzy c-means algorithm with application in MR image segmentation. *Pattern Recognition Letters*, 34(12): 1329–1338, 2013.

[28] Ahmed Nasreddine Benaichouche, Hamouche Oulhadj, and Patrick Siarry. Improved spatial fuzzy c-means clustering for image segmentation using PSO initialization, mahalanobis distance and post-segmentation correction. *Digital Signal Processing*, 23(5): 1390–1400, 2013.

[29] S.R. Kannan, R. Devi, S. Ramathilagam, and K. Takezawa. Effective FCM noise clustering algorithms in medical images. *Computers in biology and medicine*, 43(2): 73–83, 2013.

[30] Liang Liao and Tu-Sheng Lin. A fast spatial constrained fuzzy kernel clustering algorithm for MRI brain image segmentation. In *2007 International Conference on Wavelet Analysis and Pattern Recognition*, volume 1, pages 82–87. IEEE, 2007.

[31] D. Selvathi and R. Dhivya. Segmentation of tissues in MR images using modified spatial fuzzy c means algorithm. In *2013 International Conference on Signal Processing, Image Processing & Pattern Recognition*, pages 136–140. IEEE, 2013.

[32] Sudip Kumar Adhikari, J.K. Sing, D.K. Basu, M. Nasipuri, and P.K. Saha. Segmentation of MRI brain images by incorporating intensity inhomogeneity and spatial information using probabilistic fuzzy c-means clustering algorithm. In *2012 International Conference on Communications, Devices and Intelligent Systems (CODIS)*, pages 129–132. IEEE, 2012.

[33] Ilya Levner and Hong Zhang. Classification-driven watershed segmentation. *IEEE Transactions on Image Processing*, 16(5): 1437–1445, 2007.

[34] Varshika Pandey and Vipin Gupta. MRI image segmentation using Shannon and Non-Shannon entropy measures. *International Journal of Application or Innovation in Engineering & Management*, 3(7): 41–46, 2014.

[35] M. Stella Atkins and Blair T. Mackiewich. Fully automatic segmentation of the brain in MRI. *IEEE transactions on medical imaging*, 17(1): 98–107, 1998.

[36] Samy Sadek and Sayed Abdel-Khalek. Generalized [alpha]-entropy based medical image segmentation. *Journal of Software Engineering and Applications*, 7(1): 62, 2014.

[37] Chun Yuan and Shangli Liang. Segmentation of color image based on partial differential equations. In *2011 Fourth International Symposium on Computational Intelligence and Design*, volume 2, pages 238–240. IEEE, 2011.

[38] H. Sen and A. Agarwal. A comparative analysis of entropy based segmentation with Otsu method for gray and color images, *2017 International conference of Electronics, Communication and Aerospace Technology (ICECA)*, pages 113–118, IEEE, 2017.

[39] Brainweb: Simulated brain database. [Online; accessed 17th September, 2018].

[40] The Internet Brain Segmentation Repository (IBSR). [Online: accessed 25th November, 2018].

[41] Chris A. Cocosco, Vasken Kollokian, Remi K-S Kwan, G. Bruce Pike, and Alan C. Evans. Brainweb: Online interface to a 3D MRI simulated brain database. In *NeuroImage*. Citeseer, 1997.

[42] James C. Bezdek. Cluster validity with fuzzy sets. 1973.

[43] James Bezdek. Mathematical models for systematics and taxonomy. 01 1975.

[44] Nikhil R. Pal, Kuhu Pal, James M. Keller, and James C. Bezdek. A possibilistic fuzzy c-means clustering algorithm. *IEEE transactions on fuzzy systems*. 13(4), 517–530, 2005.

[45] J. C. Dunn. A Fuzzy Relative of the ISODATA Process and Its Use in Detecting Compact Well-Separated Clusters, *Journal of Cybernetics*, 3:3, 32–57, 1973.

[46] C. E. Shannon, A mathematical theory of communication, in *The Bell System Technical Journal*, 27(3):379-423, 1948.